https://doi.org/10.5194/egusphere-2023-2218
Preprint. Discussion started: 16 October 2023

Influence of Cloud Retrieval Errors Due to Three Dimensional Radiative Effects on Calculations of Broadband Cloud Radiative Effect

Adeleke S. Ademakinwa[1,2], Zahid H. Tushar[3], Jianyu Zheng[1,2], Chenxi Wang[2,4], Sanjay Purushotham[3], Jianwu Wang[3], Kerry G. Meyer[4], Tamas Várnai[2,4], Zhibo Zhang[1,2,*]

1. Physics Department, University of Maryland Baltimore County (UMBC)
2. Goddard Earth Sciences Technology and Research (GESTAR) II, UMBC
3. Department of Information Systems, UMBC
4. Climate and Radiation Laboratory Code 613, NASA Godard Space Flight Center

*Corresponding author: Zhibo Zhang, zhibo.zhang@umbc.edu

https://doi.org/10.5194/egusphere-2023-2218
Preprint. Discussion started: 16 October 2023

Abstract

We investigate how cloud retrieval errors due to the three-dimensional (3D) radiative effects affect broadband cloud radiative effects (CRE). A framework based on the combination of large eddy simulations (LES) and radiative transfer (RT) models was developed to simulate both one-dimensional (1D) and 3D radiance, and shortwave (SW) broadband fluxes. Results show that the broadband SW fluxes reflected at top-of-the-domain, transmitted at the surface, and absorbed in the atmosphere, computed from the cloud retrievals using 1D-RT (called "1D-RT+retrieved clouds") can provide reasonable broadband radiative energy estimates in comparison with those derived from the true cloud fields using 1D-RT (called "1D-RT+true clouds"). The difference between these 1D-RT simulated fluxes (1D-RT+retrieved clouds simulations, 1D-RT+true clouds simulations) and the benchmark 3D-RT simulations from the true cloud field (called "3D-RT+true clouds"), depends primarily on the horizontal transport of photons in 3D-RT, whose characteristics vary with the Sun's geometry. When the solar zenith angle (SZA) is 5°, the domain-averaged fluxes simulated based on the 1D-RT+retrieved clouds are in excellent agreement with the 3D-RT+true clouds results, all within 7% relative CRE bias. When the SZA is 60°, the differences between the results from the 1D-RT+retrieved clouds and 3D-RT+true clouds are determined by how the cloud side-illumination and shadowing effects offset each other in the radiance, retrieval, and broadband fluxes. This study suggests that although the cloud property retrievals based on the 1D-RT theory may be biased due to the 3D radiative effects, they still provide an observational basis for the estimation of broadband fluxes.

https://doi.org/10.5194/egusphere-2023-2218
Preprint. Discussion started: 16 October 2023

1. Introduction

Covering about 60-70% of the Earth's surface [Rossow and Schiffer, 1999; Vardavas and Taylor, 2011], clouds play a very important role in the Earth's climate system. Clouds can cool the Earth by reflecting shortwave (SW) solar radiative flux back to space and at the same time warm the Earth by retaining the outgoing longwave (LW) infrared radiative flux at the top of the atmosphere (TOA), known as the cloud radiative effects (CRE). The annual global average TOA CRE is approximately $-50\ \mathrm{Wm^{-2}}$ at SW and $30\ \mathrm{Wm^{-2}}$ at LW, resulting in a net CRE of about $-20\ \mathrm{Wm^{-2}}$ [Intergovernmental Panel on Climate Change (IPCC) Fifth Assessment Report Chapter 7]. These strong CRE show that clouds greatly affect the Earth's energy budget [Ramanathan et al., 1989; Kiehl and Trenberth, 1997; Trenberth et al., 2009]. The CRE of clouds is largely determined by the optical and microphysical properties of clouds including the cloud optical thickness (τ), cloud droplet effective radius ($\mathrm{r_e}$), and cloud liquid water path (LWP). Thus, continuous measurements of these cloud properties from regional to global scales are critical to better understand the role of clouds in the climate systems. Currently, satellite based remote sensing is the only way to make such observations. Remotely "retrieved" cloud properties based on these satellite observations are often used to derive the radiative effects of clouds [e.g., Wielicki et al., 1996; Platnick et al., 2003; Loeb and Manalo-Smith, 2005; Oreopoulos et al., 2016] and evaluate the simulations of Earth System Models (ESMs) [Kay et al., 2012; Nam et al., 2012; Song et al., 2018].

A commonly used retrieval technique in passive satellite remote sensing is the bi-spectral retrieval method first developed by Nakajima and King [1990]. It retrieves τ and $\mathrm{r_e}$ simultaneously from a pair of total reflectance measurements, one from the non-absorbing visible or near infrared (VNIR) band (e.g., 0.66 µm) and the other from the moderately absorbing short-wave infrared (SWIR) band (e.g., 2.13µm). Since clouds in reality have three-dimensional (3D) structures, the simulation of radiative transfer (RT) in clouds should ideally consider the transport of radiation in both vertical and horizontal directions (referred to as "3D RT"). Unfortunately, the computational cost for 3D RT is extremely high. As a result, the operational bi-spectral cloud retrievals are almost exclusively based on the one-dimensional (1D) RT theory that considers only the vertical and ignores the net horizontal transport of radiation. The radiative properties of clouds under 3D RT are substantially different from those under 1D RT. This is known as the 3D radiative effects and can lead to substantial biases in the cloud property retrievals based on 1-D RT [Várnai et al., 2001; Marshak et al., 2006; Zhang et al. 2012; Zhang et al. 2016]. Although recent efforts have been made to employ machine learning techniques to retrieve cloud properties based on 3D RT theory [Okamura et al., 2017; Masuda et al., 2019], these machine-learning based algorithms are still in their infancy and far from being used in operational algorithms.

Many previous studies have investigated the 3D radiative effects on satellite radiance observations and cloud property retrievals. For example, Welch and Wielicki [1984] used some "toy" cloud fields (e.g., cubic, and cylindrical) to illustrate the impact of side-illuminating and mutual shadowing on cloud albedo. Várnai and Davis [1999] and Várnai [2000] elucidated several 3D RT mechanisms, e.g., upward/downward trapping/escaping, that can result in significant differences between 1D and 3D cloud albedo. Davis and Marshak [2001] pointed out that the channeling effect in 3D RT can smoothen out the small-scale cloud variations and lead to the reduction of cloud brightness at cloud edges. Marshak et al. [2006] explained how the radiance biases due to 3D radiative effects can lead to τ and $\mathrm{r_e}$ retrieval biases in MODIS (Moderate Resolution Imaging Spectroradiometer) cloud products. This study is built upon these classic papers but has a different objective.

https://doi.org/10.5194/egusphere-2023-2218
Preprint. Discussion started: 16 October 2023

Here, we investigate an important question: Do cloud property retrievals based on 1D RT, which are potentially biased due to the 3D radiative effects, still provide an observational basis to estimate the broadband CRE? This is an important question because as mentioned above, operational cloud retrieval products from, for example MODIS, are frequently used for CRE estimation and ESM evaluation. However, to our best knowledge, the impacts of retrieval bias due to the 3D radiative effects on such applications have never been examined systematically in previous studies. To better explain our objective and the difference of this study from many previous ones on the 3D radiative effects, we need to introduce a framework illustrated in **Fig. 1**. As conceptually illustrated in **Fig. 1**, the observed radiances are inherently 3D (i.e., from Box A to C) because the RT in nature is 3D. However, when 1D RT theory is used to interpret the observations, we get the "retrieved cloud properties" in Box D that can be significantly different from the "true" cloud properties in Box A. Although the retrieved cloud properties are often biased due to the 3D radiative effects, they are still widely used to compute the radiative fluxes by clouds (i.e., from Box D to E) using 1D RT and the results are often used for studying the climatic effects of clouds [e.g., Kato et al., 2011; Zelinka et al., 2012; Oreopoulos et al., 2016]. In contrast, the "true" radiative fluxes in nature are also 3D (i.e., from Box A to F). A few recent studies have computed and compared the 1D and 3D radiative fluxes and heating rates by clouds. For example, Barker et al. [2011, 2012] and more recently Okata et al. [2017] compared the 1D and 3D SW fluxes computed based on the constructed A-Train cloud scenes at the TOA and surface. The main difference between their study and this current work is as follows: They compared the 3D (i.e., Box F in **Fig. 1**) with the 1D broadband fluxes (i.e., Box G in **Fig. 1**) both computed from the "true" clouds. In contrast, we argue that the "true" clouds are not known in practice and therefore it is more reasonable to compare the 3D flux (i.e., Box F in **Fig. 1**) with the 1D flux computed from the "retrieved cloud properties" (i.e., Box E in **Fig. 1**).

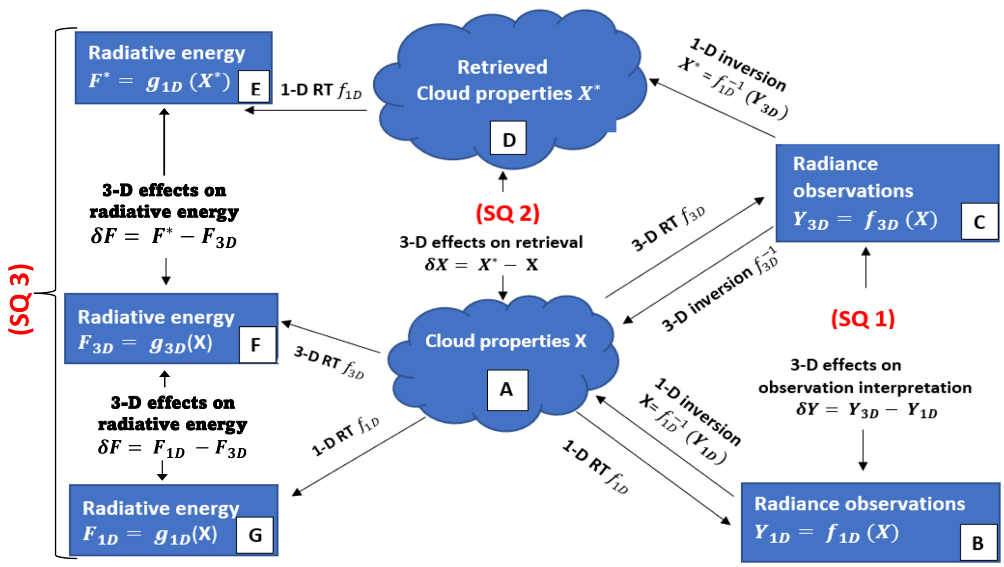

Fig. 1. Conceptual framework to understand the study.

https://doi.org/10.5194/egusphere-2023-2218
Preprint. Discussion started: 16 October 2023

The above analysis of **Fig. 1** reveals a big uncertainty in the current studies of CRE, i.e., we know the retrieved cloud properties are biased due to the 3D radiative effects but still have to use them for the CRE computations. This raises a highly important question: Do cloud property retrievals based on 1D RT, which are potentially biased due to 3D radiative effects, still provide an observational basis to estimate the broadband CRE? This question motivates this study and will focus on the three important scientific questions (SQs) in the framework illustrated in **Fig. 1**:

- SQ1: How does the radiance simulated based on 3D RT model compare with the 1D results for different types of clouds at different illuminating-viewing geometries? (i.e., Comparing Box C to B in **Fig. 1**).
- SQ 2: How does the "retrieved cloud properties", e.g., τ and r_e, derived based on the 3D radiance field using 1D RT, compare to the "true" cloud properties? (i.e., Comparing Box D to A in **Fig. 1**).
- SQ 3: How are the broadband SW radiative fluxes derived from the retrieved cloud properties (using 1D RT) different from the "true" radiative fluxes (computed from the "true" cloud fields using 3D RT) ? And how does this result compare with the difference between the broadband SW radiative fluxes computed from the "true" cloud properties using 1D RT and those computed from the "true" cloud properties but using 3D RT? (i.e., Comparing Box F to E and G in **Fig. 1**).

The paper's remaining structure is arranged as follows: Section 2 briefly describes the data and theory for the study. Section 3 presents and discusses results on how the 3D radiative effects influences the radiance fields, cloud property retrievals and broadband radiative flux. The summary and conclusion are given in Sect. 4.

2. Data and Theory

2.1. Cloud field data set

A great challenge facing 3D radiative effects studies is that the "true" clouds are always obscured by the 3D radiative effects which are inevitable in real observations. To overcome this challenge, many previous studies [e.g., Zhang et al., 2012; Miller et al., 2017; Rajapakshe and Zhang, 2020] have used synthetic cloud fields and RT simulations to mimic the observation-retrieval process and study the 3D radiative effects. Building on these previous studies, we adopt the same state-of-the-art satellite retrieval simulator by Zhang et al. [2012] and added a broadband flux computation function to study the 3D radiative effects and its impact on broadband SW radiative flux. As described in Zhang et al. [2012] and illustrated in **Fig. 1**, the framework consists of three major components: 1) Synthetic cloud fields; 2) RT models (for radiance and broadband flux simulations); 3) cloud property (e.g., τ and r_e) retrieval simulator. Similar to Zhang et al. [2012], the synthetic cloud fields utilized in this study are based on Large--Eddy Simulations (LES) cloud fields.

Since the 3D radiative effects on overcast clouds are minimal, two cloud fields of low and intermediate cloud fractions have been selected as a case study to illustrate the framework explained in Sect. 1. The selected cloud fields were from the LES Atmospheric Radiation Measurement (ARM) Symbiotic Simulation and Observation (LASSO) Activity, conducted in the ARM Southern Great Plain (SGP) site located in Lamont, Oklahoma [Gustafson et al., 2020] (https://www.arm.gov/capabilities/modeling/lasso/). LASSO enhances ARM's observations by using LES modeling to provide contextual and self-consistent representation of the atmosphere surrounding the ARM site. It also provides continuous observations from ground-based cloud and radiometric instruments

https://doi.org/10.5194/egusphere-2023-2218
Preprint. Discussion started: 16 October 2023

which is valuable for enhancing research on cloud-radiation interactions. For this study, the two snapshots of LASSO LES cloud field cases analyzed are: 14:00 UTC on June 27 June 2015, simulation ID=108 [ARM user facility, 2015] and the other at 14:00 UTC on 18 August 2016, simulation ID=113 [ARM user facility, 2016]. For conciseness in this text, these snapshots will be referred to as "27 June" and "18 August" respectively. We chose to use these specific LASSO LES cloud fields data from the stated dates, because it represents typical shallow cumulus clouds, does not contain ice (to avoid the complexities dealing with ice microphysics) and has better diagnostic statistics compared to other LES data streams.

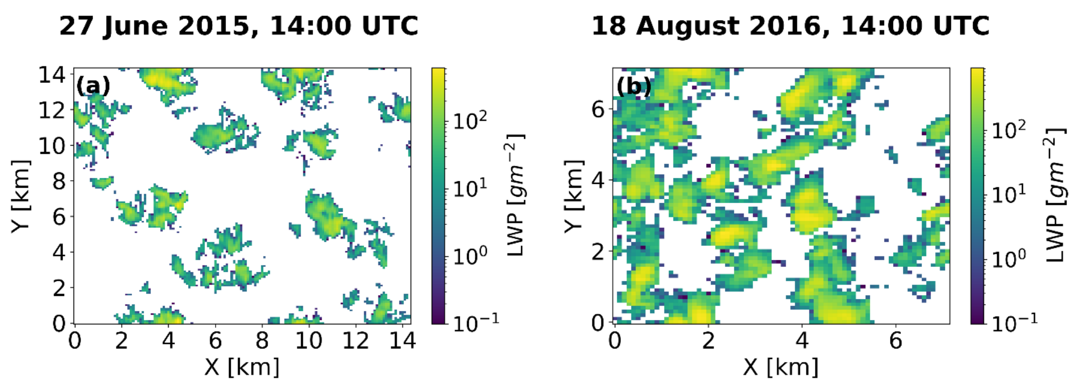

Fig. 2. Large-Eddy Simulation **(**LES) of cloud liquid water path (LWP) for 14:00 UTC, 27 June 2015 (a), and 14:00 UTC, 18 August 2016 (b) at the ARM SGP atmospheric observatory. White areas are clear-sky regions where cloud liquid water path (LWP) =0.

The LASSO LES cloud fields are characterized by broken cloud pattern spatially distributed across the domain as seen in the LWP maps in **Fig. 2a and b** for the 27 June and 18 August cases, respectively. The 3D distribution of cloud liquid water content (LWC) was obtained from the LASSO cloud fields data and a two-moment bulk microphysics scheme by Morrison et al. [2008] (see their equation 5 in Sect. 2) was used to obtain the r_e associated with the corresponding LWC distribution. It is important to note that for this study, a cloudy column has been defined as a column with LWP > 0 (i.e., clear-sky regions have LWP=0). The cloud fields have different domain sizes and microphysics distribution, and the cloud cover for the 18 August cloud field (47.08%) is more than twice that of the 27 June cloud field (20.15%). Information about the cloud properties and the LES domain are summarized in **Table 1**.

Table 1. Cloud property characteristics for the LES cloud field cases. The mean cloud effective radius (r_e), mean cloud optical thickness (τ), and In-cloud liquid water path are from the average of the cloudy regions only. The columns from left to right are case name, cloud fraction, mean In-cloud liquid water path, cloud base height (CBH), cloud top height (CTH), mean r_e, mean τ, grid spacing, and domain size, respectively.

Case name	CF (%)	Mean In-cloud LWP (gm^{-2})	CBH (km)	CTH (km)	Mean r_e (μm)	Mean τ	Grid spacing (m)	Domain size (km^3)
27 June 2015, 14:00 UTC	20.15	51.08	1.815	2.835	7.196	10.95	Δx=Δy=100,Δz=30	14.4x14.4x ~2.8

https://doi.org/10.5194/egusphere-2023-2218
Preprint. Discussion started: 16 October 2023

18 August 2016, 14:00 UTC	47.08	127.67	0.945	2.355	8.020	23.24	Δx=Δy=100,Δz=30	7.2 x7.2 x	~2.4

2.2. Radiative Transfer Setup

We use the spherical harmonics discrete ordinate method (SHDOM) RT model developed by Evans [Evans, 1998] to handle both 1D and 3D radiance computations. We have benchmarked the SHDOM simulations against the results from our previous studies [Zhang et al., 2012; Miller et al., 2016]. Broadband SW radiative flux computations, both 1D and 3D, were performed with the Intercomparison of 3D Radiation Codes (I3RC) Monte Carlo community model [Pincus and Evans, 2009], and atmospheric gaseous absorption was incorporated via the SW Rapid Radiative Transfer Model (RRTM) correlated k-distribution approach [Mlawer et al., 1997] which consists of 14 bands with spectral range from 0.2 to 12 µm (This coupled broadband radiative flux solver is hereafter known as the "I3RC+CKD" model). Rayleigh scattering was included in the flux RT calculations, the background atmospheric profiles are taken to be horizontally homogeneous throughout the domain and the profiles of atmospheric temperature, pressure, ozone, air density and the water vapor profile utilized for the RT flux calculations were obtained from the sounding data at the ARM SGP site on 27 June 2015. Ambient aerosols are neglected in the RT calculations for simplicity. The 1D broadband RT flux calculations were performed with the same I3RC+CKD model, by dividing the LES domain into individual columns and RT was calculated on each LES column properties separately and independently.

The spectral cloud optical properties were calculated using Mie scattering theory and were averaged over each RRTM spectral bands. The phase functions were represented using Legendre coefficients with 35 log spaced effective radius spanning from 2 to 40 µm. The surface was assumed to be Lambertian with surface spectral albedos obtained from ARM SGP site [Trishchenko et al., 2003] applied for wavelength (λ) in the range 0.2 ≤λ≤ 2.5 µm, while surface spectral albedo corresponding to a vegetative covered surface [Zhuravleva et al., 2009] was utilized for λ> 2.5 µm. In the Monte Carlo calculations, 10^8 and 10^4 photons were initiated for calculations of the 3D broadband SW flux and the column-independent 1D broadband SW flux, respectively. The radiative transfer calculations were implemented for two solar zenith angles (SZAs), a high Sun case with SZA of 5° and a low Sun case with SZA of 60°. In the broadband flux calculations, the downward flux at the top of the domain (TOD) corresponds to 1363 $\mathrm{Wm^{-2}}$ and 684.1 $\mathrm{Wm^{-2}}$ for SZA 5° and 60°, respectively. Throughout this study, we choose a constant 0° relative azimuth angle (RAA) and a constant 0° viewing zenith angle (VZA). The Double periodic horizontal boundary conditions were applied for all the RT calculations, and all RT calculations have been conducted at the native LES resolution of 100 m. Coarser spatial resolution will be applied in future studies.

2.3. Bi-spectral retrieval method

As introduced in Sect. 1, one of the most widely used methods for retrieving the τ and r_e is the bi-spectral retrieval technique proposed by Nakajima and King [1990]. This retrieval method uses passive remote sensing measurements of the reflection function at a pair of wavelengths, one chosen from the VNIR band where water has negligible absorption and therefore cloud absorption is more sensitive to the τ and the other wavelength is chosen from the SWIR band where water has significant absorption and

https://doi.org/10.5194/egusphere-2023-2218
Preprint. Discussion started: 16 October 2023

therefore is more sensitive to the r_e. The bi-spectral retrieval method is solely based on the 1D RT theory to interpret the observed cloud reflectance. It is implemented using a precomputed Look up table (LUT) which consists of 1D reflectance function for different τ and r_e combinations at the required solar-view geometry (an example LUT is shown in **Fig. 3**). The observed cloud reflectance is then utilized as inputs to the LUT to simultaneously retrieve the τ and r_e via a two-dimensional (2D) interpolation between the observed cloud reflectance and the LUT grid. Notably, in the bi-spectral LUT regions with smaller τ, the retrieval uncertainty increases because the isolines of the LUT τ are less orthogonal and more tightly packed. This non-linearity in the LUT has high inhomogeneity consequences for cloud retrievals at the pixel level [Zhang et al., 2012, 2016]. In this study, the VNIR reflectance were measured at 0.66 µm (identical to the central wavelength of operational MODIS retrieval algorithm over a vegetative land surface), while the SWIR reflectance were measured at the 2.13 µm wavelength. The LUT utilized for our bi-spectral retrievals have 19 effective radii spanning from 5 to 40 µm, and 43 log spaced τ values spanning from 0.05 to 158.48. While a constant effective variance (v_e) value of 0.1 is used for consistency with all other RT simulations in this study. The surface albedo in both 0.66 and 2.13 µm wavelengths for the LES radiance simulations and LUT RT calculations was 0.07. This value is consistent with the surface albedo of similar spectral bands in the broadband SW flux computations.

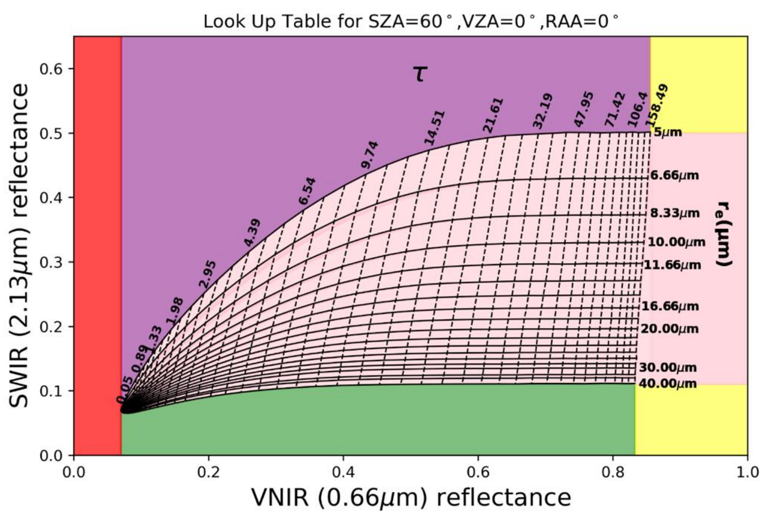

Fig. 3. An example Nakajima and King bi-spectral Look up table (LUT) space. The solid lines are the reflectance function contours for fixed cloud effective radius (r_e), while the dashed lines are for fixed cloud optical thickness (τ). Surface is Lambertian with surface albedo=0.07. The solar zenith angle (SZA) is 60°, the view zenith angle (VZA) is 0°, and the relative azimuth angle (RAA) is 0°.

2.4. Classification of failed and successful retrievals

One major challenge in cloud property retrievals from satellite remote sensing instruments like MODIS, is the so called "failed retrievals". A retrieval can be considered failed if there is no r_e and τ LUT grid combination to interpret the reflectance observation, or if there is no realistic cloud microphysics to explain the retrieved cloud property (e.g., a retrieved r_e > 40 µm). These can be due to several factors,

https://doi.org/10.5194/egusphere-2023-2218
Preprint. Discussion started: 16 October 2023

such as the limits of the LUT, clouds overlapping effect, presence of partially cloudy pixels, extreme solar-satellite viewing geometries, strategy used in cloud mask implementation and the optical characteristics of the underlying surface. Potential causes and rate of occurrence of failed MODIS retrievals for marine liquid phase clouds have been studied extensively [Cho et al., 2015]. In this study, we refer to MODIS cloud property retrieval algorithm's classification of failed retrievals [Platnick et al., 2016] and the study by Cho et al. [2015], to classify a pixel as successful or failed retrieval as explained below:

1) For observations with both VNIR and SWIR reflectance observations within the LUT solution space, the nearest interpolated τ and r_e values are retrieved (Pink area bounded by the LUT lines in **Fig. 3**). If the observed VNIR reflectance exceed the upper limit of LUT τ but within the LUT r_e solution range (extended pink area in **Fig. 3**), the nearest LUT r_e is retrieved and the maximum LUT τ value (τ=158.48) is assigned to the retrieval. These explained categories are classified as "successful retrievals" for this study.
2) In other cases, for observations with VNIR reflectance within the LUT solution space but SWIR reflectance above the LUT solution space (purple area in **Fig. 3**), the nearest τ values are retrieved but the smallest LUT r_e value of 5 μm is assigned to the retrievals. This category of retrieval failure is called "r_e too small" failures. In cases where the VNIR reflectance observations are within the LUT τ solution space, but the SWIR reflectance are below the LUT solution space (green area in **Fig. 3**) the nearest τ values are retrieved but the largest LUT r_e value of 40 μm is assigned to the retrieval. This category of retrieval failure is called the "r_e too large" failures. In cases where the observed VNIR reflectance is greater than the largest LUT τ value and the observed SWIR reflectance is smaller than the largest LUT r_e (i.e., the lower yellow region in **Fig. 3**), the retrievals are assigned the largest τ value (τ=158.48) and the largest r_e value (r_e=40 μm). For observations with VNIR reflectance greater than the largest LUT τ value and the SWIR reflectance greater than the smallest LUT r_e value (i.e., the upper yellow region in **Fig. 3**), the retrievals are assigned the largest τ value (τ=158.48) and smallest r_e value (r_e=5 μm). Lastly, for observations with VNIR reflectance below the minimum LUT τ (red area in **Fig. 3**), the r_e and τ retrievals are assigned fill values (which are represented by τ = 0 in our flux calculations). These explained categories are called "τ" failures. The r_e too small, r_e too large and τ failure categories are collectively classified as "failed retrievals" for this study.

2.5. Approach for radiative transfer simulation and result comparisons

To address the three SQs for our study (identified in Sect. 1), we performed a total of fourteen experiments for each cloud field. The first four experiments were performed with the SHDOM model to study the 3D radiative effects on radiance observation interpretation and address SQ1, it involves comparing 1D and 3D RT radiance simulations (Box B vs C depicted in **Fig. 1**) for the high and low Sun cases. The next four experiments involve comparing cloud property retrievals from 3D and 1D RT radiance observations (Box B to A vs Box D in **Fig. 1**) for both high and low Sun, to examine the influence of the 3D radiative effects on the retrieved cloud properties and address SQ2. These experiments were conducted using radiance fields as inputs to the precomputed LUT described in Sect. 2.3. The last six experiments were conducted to examine the impact of the 3D radiative effects on the broadband solar radiative flux for both high and low Sun scenarios in the LES domains and address SQ3. These experiments involve the calculation of the broadband solar radiative flux for each SZA within three distinct categories (**Table 2**). The first set of flux was computed based on the "true" cloud field and 3D RT (i.e., Box F in **Fig. 1**) hereafter referred to as the "3D-RT + true clouds" experiment. The second set was computed based on the

https://doi.org/10.5194/egusphere-2023-2218
Preprint. Discussion started: 16 October 2023

"retrieved cloud properties" using 1D RT (Box E in **Fig. 1**) hereafter referred to as the "1D-RT + retrieved clouds" experiment, and the third was computed based on the "true" cloud field and 1D RT (Box G in **Fig. 1**) hereafter referred to as the "1D-RT + true clouds" experiment. It is important to note that in the 1D-RT + retrieved clouds experiment, the retrieved cloud properties (τ and r_e) are utilized to calculate the retrieved LWP (using retrieved LWP $\cong 2\tau\rho r_e/3$, where ρ is the density of liquid water; [Stephens, 1977; Liou, 1992]) which are then reconstructed into r_e and LWC distribution for each LES column while preserving the vertical structure of the original LES cloud field. 1D RT are then performed using the reconstructed retrieved clouds as inputs to obtain the 1D-RT + retrieved clouds experiment's results. Note, unless otherwise stated, for this study, the successful and failed retrievals (as described in Sect. 2.4) have been used to represent the total population of cloudy pixels in the cloud property inputs for the 1D-RT + retrieved clouds experiment.

Table 2. Description of the Flux experiments

Name	Description
3D-RT + true clouds	Broadband SW flux computed based on "true" cloud field and 3D RT model
1D-RT + retrieved clouds	Broadband SW flux computed based on "retrieved cloud properties" and 1D RT model
1D-RT + true clouds	Broadband SW flux computed based on "true" cloud field and 1D RT model

The 1D-RT + true clouds experiment is identical to the 3D-RT + true clouds experiment except for the absence of the horizontal movement of photons between the LES grid columns. This enables us to determine the impact of neglecting the horizontal movement of photons on the broadband radiative fluxes. On the other hand, in reference to the 3D-RT + true clouds experiment, the 1D-RT + retrieved clouds experiment will not only help us to better understand the implications of neglecting the horizontal transport of photons but will also enable us to measure how biases in the retrieved cloud properties (which are affected by the 3D radiative effects) impact the broadband radiative fluxes.

In order to describe the impact of the 3D radiative effects on the radiance fields, retrieved cloud properties and broadband radiative flux, we first examine their effects across the LES domain and subsequently quantify their overall impact on the domain by computing the horizontally domain-averaged results and determine the absolute bias, hereafter referred to as "bias" for brevity and is defined as $\bar{y} - \bar{x}$, where $\bar{y}$ denotes the domain-averaged result from the 3D RT quantity (e.g., Reflectance or flux), and $\bar{x}$ denotes the domain-averaged result from the 1D RT quantity (e.g., Reflectance or flux).

To quantify the difference between the CRE computed from the benchmark 3D-RT + true clouds experiment and the CRE computed from the 1D-RT + true or 1D-RT + retrieved clouds experiment, we define a domain-scale quantity known as the relative cloud radiative effects (rCRE) bias as:

$$\text{rCRE bias} = \left(1 - \frac{\text{CRE}_{1\text{D}}}{\text{CRE}_{3\text{D}}}\right) \times 100 \quad (1)$$

Where $\text{CRE}_{1\text{D}}$ is the CRE calculated from either the 1D-RT + true clouds or the 1D-RT + retrieved clouds experiment in units of Wm^{-2} and $\text{CRE}_{3\text{D}}$ is the CRE calculated from the 3D-RT + true clouds experiment in units of Wm^{-2}. According to this definition, a rCRE bias of 0% would indicate that there is no bias

https://doi.org/10.5194/egusphere-2023-2218
Preprint. Discussion started: 16 October 2023

between the CRE computed from the 1D-RT + true clouds or 1D-RT + retrieved clouds experiments and the CRE computed from the 3D-RT + true clouds experiment (i.e., the CRE computed from the 1D-RT + true or 1D-RT + retrieved clouds experiment is equivalent to the CRE computed from the 3D-RT + true clouds experiment), while a positive rCRE bias value greater than 0% would quantify the percentage by which the CRE computed from the 1D-RT + true clouds or 1D-RT + retrieved clouds experiment is lesser than the CRE computed from the 3D-RT + true clouds experiment and thus indicate that the 1D experiment underestimate the CRE relative to the 3D-RT + true clouds experiment. Also, a negative rCRE bias value less than 0% would quantify the percentage by which the CRE computed from the 1D-RT + true clouds or 1D-RT + retrieved clouds experiment exceeds the CRE computed from the 3D-RT + true clouds experiment and imply that the 1D experiment overestimate the CRE relative to the 3D-RT + true clouds experiment.

3. Results and discussion

3.1. Investigating the 3D radiative effects on simulated radiances

Focusing first on SQ 1, we compare the reflectance obtained from the 1D and 3D RT simulations to assess the impact of the 3D radiative effects on the reflectance radiation field, i.e., Box B vs. Box C in the framework of **Fig. 1**. Specifically, we will investigate the differences in the reflectance simulated based on 3D and 1D RT ($\mathrm{R}^{3\mathrm{D}-1\mathrm{D}}$) at the two λ ($0.66$ and $2.13\ \mu\mathrm{m}$) required for our bi-spectral retrieval for both low Sun (SZA 60°) and high Sun (SZA 5°) cases. To describe the 3D radiative effects on the observed reflectance, classifications are made based on the increase in the brightness of a pixel in the LES domain. A pixel in the LES domain is considered “illuminated” ("shadowed”) if its 3D RT-based reflectance is higher (lower) than its 1D counterpart.

The $0.66\ \mu\mathrm{m}$ reflectance of the two cloud cases, based on 3D and 1D RT, and their differences are shown in **Fig. 4** for the low sun condition and in **Fig. 5** for the high sun condition. In the low Sun case, the 3D RT-based simulated reflectance maps (**Fig. 4a** for the 27 June case and **Fig. 4d** for the 18 August case) demonstrate the distinct presence of cloud shadows projected onto the clear-sky located on the opposite cloud side and opposite to the Sun’s position located on the left of the domain. These features are absent in the 1D RT-based simulated reflectance (**Fig. 4b, e**) because the radiation-cloud interactions in the 1D reflectance field is dictated by the 1D RT theory, whereby the RT in each column is independent of the surrounding column and thus the cloud shadow is cast directly beneath the cloud. Similar reflectance characteristics are observed in the simulated 1D and 3D reflectance for the SWIR band (not shown). The deviation of the 1D RT-based simulated reflectance from the 3D RT-based simulated reflectance leads to $\mathrm{R}_{\lambda}^{3\mathrm{D}-1\mathrm{D}}$ with distinct pattern of illumination and shadowing observed in some pixels across the LES domain for both the VNIR and SWIR bands ($\mathrm{R}_{\lambda=0.66\ \mu\mathrm{m}}^{3\mathrm{D}-1\mathrm{D}}$ shown in **Fig. 4c** and **f**). A closer examination of the reflectance within cloudy regions in the low Sun case for the two cloud fields reveals a consistent pattern; the illuminated pixels, where $\mathrm{R}_{\lambda=0.66\ \mu\mathrm{m}}^{3\mathrm{D}-1\mathrm{D}}$ is positive, are predominantly observed in sunlit regions that directly face the Sun (e.g., X=3.5 km, Y=14 km in **Fig. 4c**). On the other hand, shadowed pixels, where $\mathrm{R}_{\lambda=0.66\mu\mathrm{m}}^{3\mathrm{D}-1\mathrm{D}}$ is negative, are observed on the opposite side of the cloud layer (e.g., at X=5 km, Y=14 km in **Fig. 4c**). These findings are consistent with previous 3D radiative effects studies for oblique solar geometry [e.g., Várnai and Davies, 1999; Várnai, 2000; Marshak et al., 2006]. The observed opposing effects of illuminating and shadowing in the low Sun angle case does not only depend on the orientation of the cloud towards or away from the Sun, other factors like cloud-cloud interactions, cloud geometry and

https://doi.org/10.5194/egusphere-2023-2218
Preprint. Discussion started: 16 October 2023

aspect ratio, spatial distribution of the cloud in the domain and the horizontal transport of photons also contribute to these behaviors [Várnai and Marshak, 2001, 2002; Marshak and Davis, 2005; Marshak et al., 2006; Zhang et al., 2012].

In the case of the high Sun, the Sun is almost perpendicular (at SZA 5°), and its radiation interaction with clouds under 3D RT is different from that of the low Sun case. In 3D RT, when photons from the high Sun strikes a cloud, some photons are scattered and some leak from optically thick to optically thin cloudy regions and even out of the cloud layer [O'Hirok and Gauiter, 1998]. These leaking results in the darkening of the thick clouds and brightening of the surrounding thin clouds (**Fig. 5a, d**). Due to the absence of the photon leaking/darkening in the 1D RT, the 1D RT-based simulated reflectance (**Fig. 5b, e**) appear brighter than its 3D counterpart. Hence, results in negative $\mathrm{R}_{\lambda=0.66\,\mu\mathrm{m}}^{3\mathrm{D}-1\mathrm{D}}$ in the LES domain (**Fig. 5c** and **f**). The darkening characteristics is more pronounced in the 18 August case because it consists of a larger distribution of thicker clouds compared to the 27 June cloud field; large number of photons leaking from optically thicker clouds results in more significant reduction in the reflectance values and more prominent darkening effect than photons leaking from optically thinner clouds. Similar findings regarding the darkening characteristics are observed for the 2.13 µm band, although these specific results are not depicted in the figures presented.

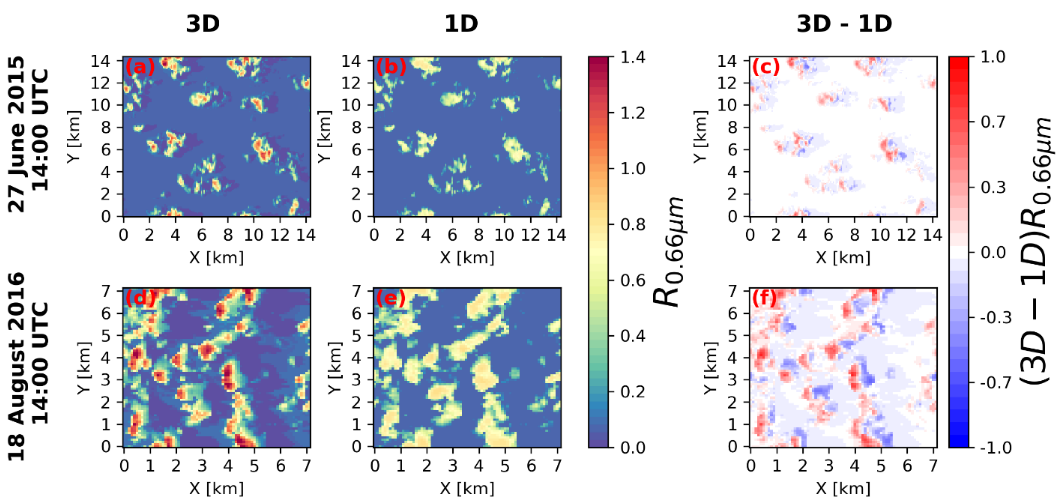

Fig. 4. Maps of the simulated 3D (a and d) and 1D (b and e) VNIR reflectance for the 27 June, and 18 August cases. Reflectance bias (3D-1D) are shown in (c) and (f) for the 27 June and the 18 August cases respectively. The direction of view is at nadir. The SZA is 60 degrees , and the Sun is at the left of the domain.

https://doi.org/10.5194/egusphere-2023-2218
Preprint. Discussion started: 16 October 2023

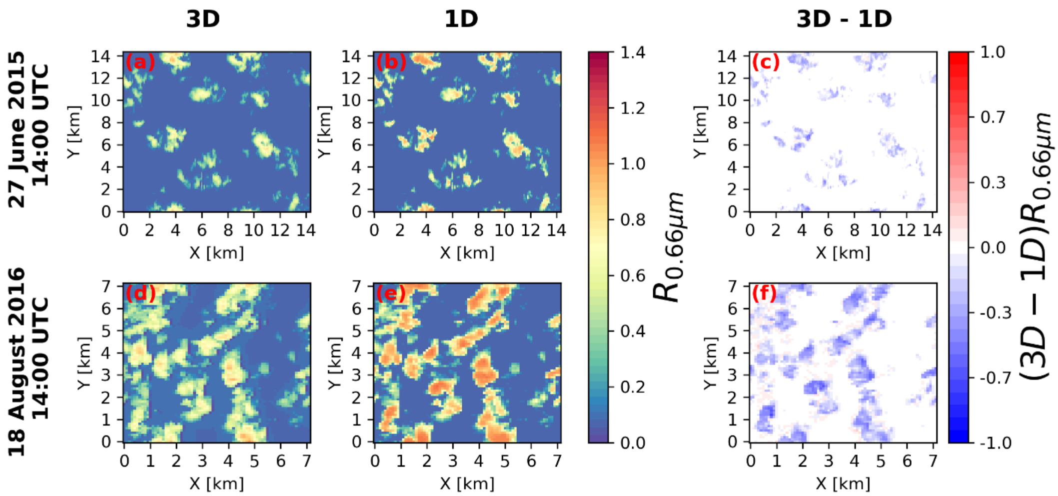

Fig. 5. Maps of the simulated 3D (a and d) and 1D (b and e) VNIR reflectance for the high Sun case (SZA=5 degrees) for the 27 June and 18 August 2016, 14:00 UTC cases. Reflectance bias (3D -1D) are shown in (c) and (f) for the 27 June and the 18 August cases respectively. The direction of view is at nadir. The Sun is almost perpendicular to the domain but slightly tilted to the left.

To examine the statistical characteristics of the reflectance bias in the LES domain, the probability density function (PDF) of the reflectance bias for "cloudy only" pixels are analyzed to investigate the 3D radiative effects on the observed cloud reflectance. Subsequently, we compared this PDF to that of the reflectance bias for both "cloudy and clear-sky" pixels (i.e., the whole LES domain) to highlight the effects of cloud presence on the overall reflectance bias within the LES domain.

The PDFs of $\mathrm{R}_{\lambda}^{3\mathrm{D}-1\mathrm{D}}$ for cloudy only pixels in the low Sun case (broken black and gray lines in **Fig. 6**a, b) are characterized by positive and negative distribution in both VNIR and SWIR bands (corroborating the illuminating and shadowing effects in **Fig. 4c, f**). The overall positive reflectance bias observed in the VNIR and SWIR bands (domain mean reflectance bias of 0.0351 (0.0292) for the VNIR (SWIR) band in the 27 June case and 0.0379 for the VNIR band in the 18 August case) indicates that the illumination effects is predominant when only cloudy pixels are considered. Meanwhile, a negative SWIR reflectance bias of −0.0233 is observed in the 18 August case. This negative reflectance bias is due to more photons being trapped in the 3D RT reflectance (likely due to its larger droplet sizes absorbing more photons) than in the 1D RT which does not allow for horizontal photon transport. On the other hand, the PDFs of $\mathrm{R}_{\lambda}^{3\mathrm{D}-1\mathrm{D}}$ for the cloudy and clear-sky pixels (broken black and gray lines in **Fig. 6c, d**) is almost similar to that of the cloudy only but shows a shift of the distribution leftwards, almost centered around zero. This is expected because clear-sky regions not in the vicinity of any clouds exhibit negligible 3D radiative effects, which causes the distribution to shift closer to zero, since the cloud fraction for both cloud cases is less than 50 %. The horizontal movement of photons from cloudy to surrounding clear-sky regions increase the 3D reflectance of clear-sky areas around the sunlit cloudy regions but the strong shadowing effects on the clear-sky region located opposite the sunlit direction dominates the clear-sky only areas, and results in a

https://doi.org/10.5194/egusphere-2023-2218
Preprint. Discussion started: 16 October 2023

negative mean bias when the reflectance of clear-sky only pixels are examined. Interestingly, the mean reflectance bias for the cloudy and clear-sky pixels are of the same sign with the cloudy only values, these indicates that the cloudy pixels have significant effect on the domain-scale statistics.

The PDFs of R_{λ}^{3D-1D} in the case of the high Sun for cloudy only pixels show a larger distribution of pixels with positive R_{λ}^{3D-1D} in both the VNIR and SWIR band accompanied by longer tails to the left (red and blue solid lines in **Fig. 6a, b**). However, the reflectance bias for both cloud cases present negative values in the VNIR and SWIR bands. These observations suggest that large radiation/photos leak from a small number of thick cloud pixels to a larger number of thin clouds. This phenomenon therefore increases the number of thin clouds with positive reflectance bias, although of very small magnitude when compared to the negative biases.

Similar to the low Sun case, the PDF of R_{λ}^{3D-1D} when both cloudy and clear-sky pixels for the high Sun case are considered (red and blue solid lines in **Fig. 6c, d**), shows a significant distribution of values close to zero. Due to the leaking of photons from thick clouds to thin clouds and clear-sky regions surrounding the clouds, there is an increase in the 3D reflectance of clear-sky regions. Additionally, when the Sun is high at SZA of 5°, there are very minimal shadows cast on the clear-sky regions. These two highlighted reasons result in a positive reflectance bias for the clear-sky only region. Thus, the negative value of the cloudy and clear-sky reflectance bias (same sign as the cloudy only) indicates that the domain scale reflectance bias is dominated mainly by the cloudy only pixels and they play a significant role in the domain-scale statistics.

https://doi.org/10.5194/egusphere-2023-2218
Preprint. Discussion started: 16 October 2023

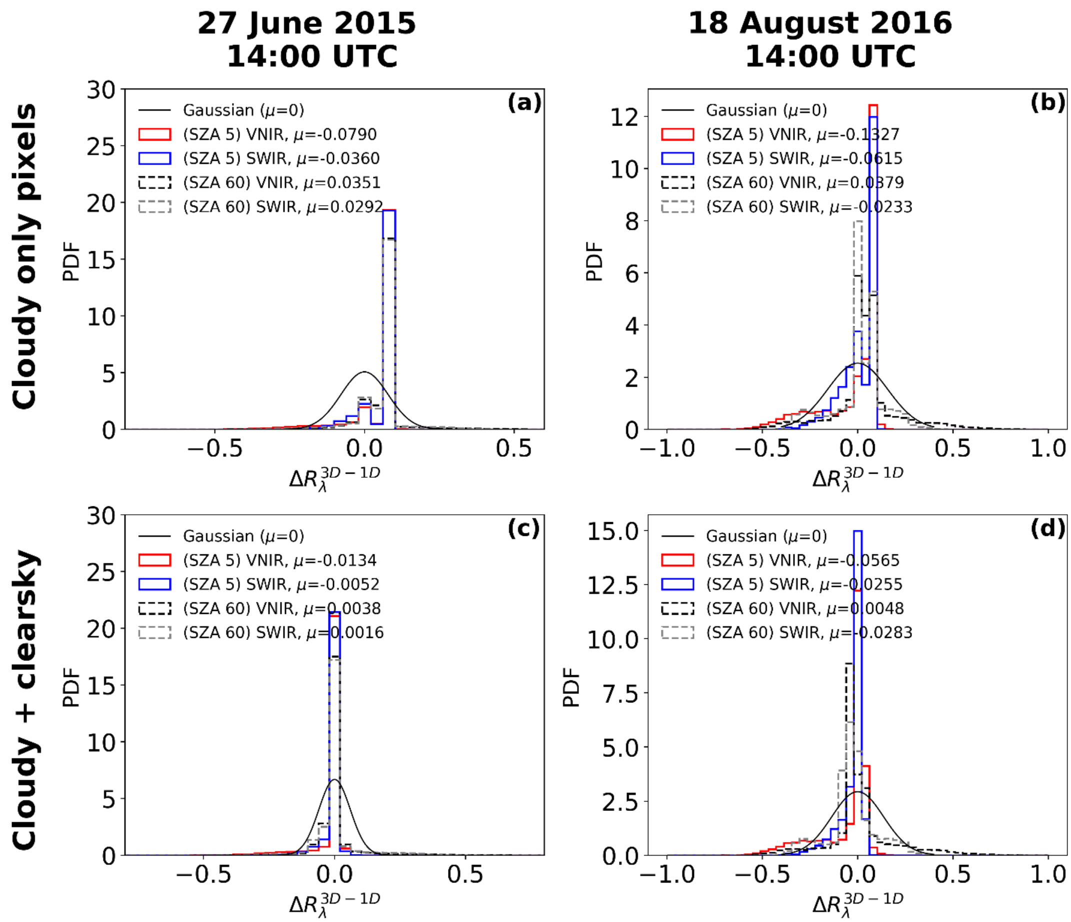

Fig. 6. PDF (Probability density function) of reflectance bias ($\Delta R^{(3D-1D)}$) for cloudy only pixels for the 27 June case (a) and 18 August case (b). PDF of reflectance bias for cloudy and clear-sky pixels for the 27 June case (c) and 18 August case (d). μ is the domain mean reflectance bias. A gaussian distribution (solid black curve) centered around zero is shown in all panels.

3.2. Investigating the 3D radiative effects on cloud retrievals

Focusing on SQ 2 in this section, we investigate how the reflectance bias, as discussed in the previous section, affect r_e and τ retrievals (i.e., Box A vs. Box D in the framework of **Fig. 1**). We utilize the 1D RT-based simulated reflectance as inputs for the LUT (explained in Sect. 2.3) to retrieve the 1D RT-based cloud droplet effective radius ($r_e^{1D\ based}$) and cloud optical thickness ($\tau^{1D\ based}$). Additionally, we use the 3D RT-based simulated reflectance as inputs for the LUT to retrieve the 3D RT-based cloud droplet effective radius ($r_e^{3D\ based}$) and cloud optical thickness ($\tau^{3D\ based}$).

https://doi.org/10.5194/egusphere-2023-2218
Preprint. Discussion started: 16 October 2023

Before discussing analysis of the 3D and 1D RT-based retrievals comparison, we first check the accuracy of our retrievals by comparing the original LES cloud properties with our 1D RT-based retrievals (i.e., comparing retrievals from 1D radiance in Box C with cloud properties in Box A in **Fig. 1**). For this purpose, the τ from the original LES (τ^{true}) is the vertical integration of the visible (0.66 μm) extinction coefficient of each column from cloud base to cloud top. For the LES r_e, we follow Zhang et al. [2017] analytical vertical weighting function (see their equation 4) to get the vertically weighted cloud droplet effective radius (r_e^{VW}) where the $\mu_o = 0.5$, μ=1 and the vertically weighting function parameter (b) associated with the 2.13 μm band was set to 2 to allow for a deeper penetration depth and for better correlation between the $r_e^{\mathrm{VW}}(2.13\ \mu\mathrm{m})$ and bi-spectral retrievals.

Fig. 7 shows the comparison between the $r_e^{\mathrm{VW}}(2.13\ \mu\mathrm{m})$ and the $r_e^{\mathrm{1D\ based}}$ as well as τ^{true} with the $\tau^{\mathrm{1D\ based}}$ for the two cloud fields at SZA=60° and VZA=0°. For this comparison, the mean τ and r_e biases are $\mu_{\tau\ \mathrm{bias}} = \langle \tau^{\mathrm{1D\ based}} - \tau^{\mathrm{true}} \rangle$ and $\mu_{r_e\ \mathrm{bias}} = \langle r_e^{\mathrm{1D\ based}} - r_e^{\mathrm{VW}}(2.13\ \mu\mathrm{m}) \rangle$

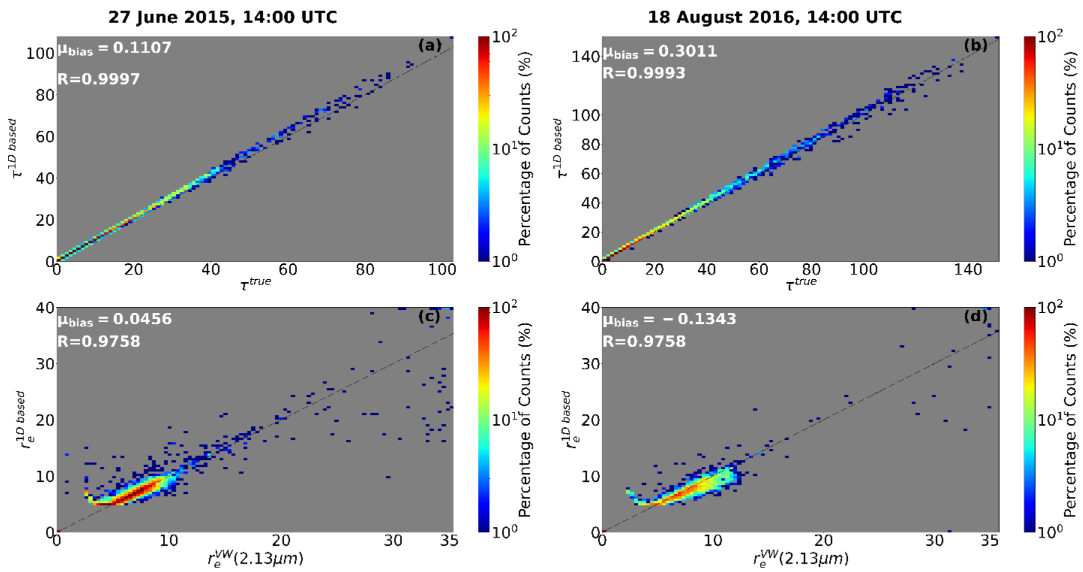

Fig. 7. Joint histogram of bi-spectral retrieved τ based on 1D RT simulated reflectance $\tau^{1D\ based}$ vs Vertically integrated τ (τ^{true}) for the 27 June case (a) 18 August case (b). Joint histogram of bi-spectral retrieved r_e based on 1D RT simulated total reflectance ($r_e^{1D\ based}$) vs vertically weighted cloud effective radius ($r_e^{vw}(2.13\mu m)$) in (c) and (d). $\mu_{bias} = \langle retrieved\ cloud\ property - reference\ cloud\ property \rangle$.

For the two cloud fields considered in this study, the $\tau^{\mathrm{1D\ based}}$ is highly correlated with the τ^{true} as seen in the joint histogram plots (**Fig. 7a** and **b**) with a correlation coefficient (R) of 0.9997 for the 27 June case, and a R of 0.9993 for the 18 August case, although both have a slight positive mean bias ($\mu_{\tau\ \mathrm{bias}} = 0.1107$ and 0.3011 for the 27 June and 18 August cases respectively). Also, the comparisons of the $r_e^{\mathrm{1D\ based}}$ with the $r_e^{\mathrm{VW}}(2.13\ \mu\mathrm{m})$ in **Fig. 7c** and **d**, shows good correlation (R > 0.96) for both cloud cases, and slightly positive mean biases ($\mu_{r_e\ \mathrm{bias}} = 0.0456$) for the 27 June case and a negative mean bias ($\mu_{r_e\ \mathrm{bias}} = -0.1343$) for the 18 August case. Certain extreme outliers bias is observed in the r_e comparisons, these outliers are attributed to thin clouds and have been studied by Miller et., al [2017].

https://doi.org/10.5194/egusphere-2023-2218
Preprint. Discussion started: 16 October 2023

Several studies [e.g., Miller et al., 2016, 2017; Zhang et al., 2012] have investigated the accuracy of 1D bi-spectral retrievals compared to vertically weighted retrievals as well as the impact of cloud vertical profile on bi-spectral retrievals. Since we have good agreement between retrievals from the 1D RT-based reflectance and the original LES cloud field properties, this study will use the $r_e^{1D\ based}$ and $\tau^{1D\ based}$ as the reference cloud properties and directly compare them with the $r_e^{3D\ based}$ and $\tau^{3D\ based}$ to investigate the impacts of the 3D radiative effects on the retrievals.

For the high Sun case, under 3D RT, photons leaking from optically thick regions to optically thin cloudy regions make the 3D radiance field to appear darker than its 1D counterpart. Consequently, for retrievals, the reflectance observation on the LUT space shifts leftwards and downwards. Thereby, larger $r_e^{3D\ based}$ are retrieved and the retrieved $\tau^{3D\ based}$ are smaller. These overestimation of the $r_e^{3D\ based}$ and underestimation of the $\tau^{3D\ based}$ retrievals is evident in the joint histogram plots of the r_e biases ($r_e^{3D\ based-\ 1D\ based}$) against the τ biases ($\tau^{3D\ based-1D\ based}$) for the two cloud fields considered in this study. In **Fig. 8a** and **b** for the 27 June and 18 August cases respectively, we observe that a larger portion of the retrievals bias falls in the third quadrant (anticlockwise starting from bottom right quadrant) where the τ bias is negative (underestimation of $\tau^{3D\ based}$) and r_e bias is positive (overestimation of $r_e^{3D\ based}$).

For the retrievals from the low Sun case, under 3D RT, it is generally observed that the sunlit optically thick cloud regions experiences illuminating effects. In the LUT solution space, illumination phenomena will shift the observed reflectance upwards and rightwards where the LUT r_e grid isolines represents smaller droplets sizes and the LUT τ isolines represents thicker clouds. Thus, $\tau^{3D\ based}$ are larger and $r_e^{3D\ based}$ are smaller than their 1D counterpart (as seen in the first bottom right quadrant in **Fig. 8c** and **d** for the 27 June and 18 August cases respectively). If a pixel is shadowed, the reflectance observation on the LUT solution space will shift downwards and leftwards to regions where the LUT r_e grid isolines represent larger droplet sizes and the LUT τ isolines represents thinner clouds. These leads to larger $r_e^{3D\ based}$ while the $\tau^{3D\ based}$ are underestimated compared to its 1D counterpart (as seen in the third quadrant anticlockwise from the bottom right in **Fig. 8c** and **d** for the 27 June and 18 August cases respectively). τ and r_e retrieval biases in satellite observations have been investigated in numerous studies [e.g., Marshak et al., 1995; Várnai and Marshak, 2002; Zhang and Platnick, 2011; Zhang et al., 2011, 2012], and in common occurrence, overestimation of the retrieved τ is coupled with the underestimation of the retrieved r_e and vice versa.

https://doi.org/10.5194/egusphere-2023-2218
Preprint. Discussion started: 16 October 2023

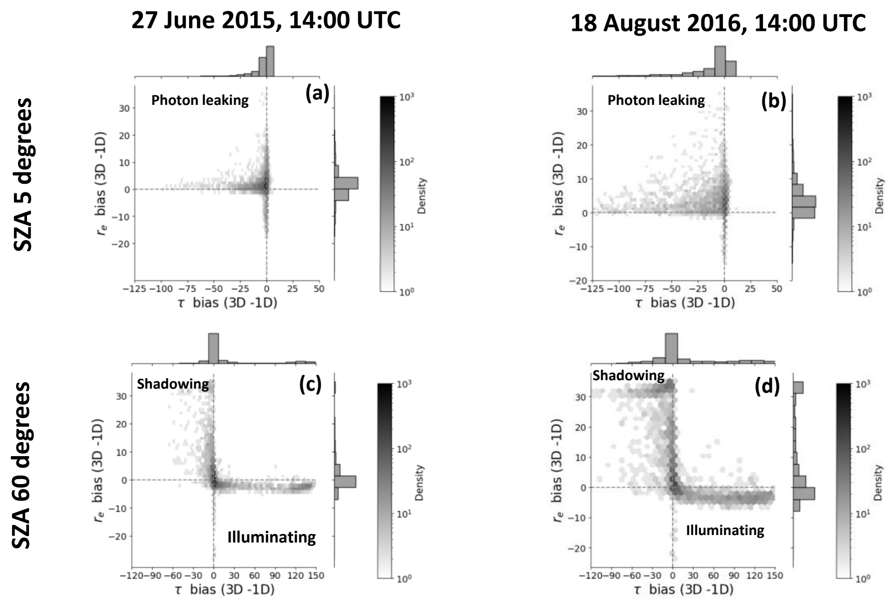

Fig. 8. Bias in cloud effective radius (r_e) against bias in cloud optical thickness (τ) retrievals for Solar zenith angle (SZA) 5 degrees for (a) the 27 June and (b) 18 August case. Bias in r_e against bias in τ retrievals for SZA 60 degrees for (c) the 27 June and (d) 18 August case.

Table 3 shows the frequency of failed and successful retrievals from 3D RT-based simulated reflectance observation for the two cloud fields considered in this study. It is observed that the number of failed retrievals is small for the SZA 5° case, while the retrieval failures are larger for the SZA 60° case for both cloud fields under consideration. This is due to a significant number (> 40 %) of the VNIR-SWIR reflectance observations falling outside the LUT solution space when the Sun is low. Conversely, the small retrieval failure rates (< 13 %) for the high Sun case is because most of the VNIR-SWIR reflectance observation (> 85 %) falls within the LUT solution space.

Table 3. Statistics of successful and failed retrievals from the 3D based radiance for the 27 June and 18 August cloud fields at Solar zenith angle (SZA) 5 and 60 degrees. The columns from left to right are Case name (Identified by date and time), solar zenith angle (SZA), Number of pixels with successful retrievals only, Pixels with failed retrievals, Total number of successful and failed retrievals.

Case name	SZA	No of pixels with successful retrievals only	Pixels with failed retrievals			Total number of successful and failed pixels
			Category of failed retrievals	No of pixels	Total	
27 June 2015, 14:00 UTC	5^o	3670 (87.82 %)	r_e *too large*	85 (2.03 %)	509 (12.17%)	4179 (100 %)
			r_e *too small*	365 (8.73 %)		
			τ *failures*	63 (1.41 %)		
	60^o	2100 (50.16%)	r_e *too large*	97 (2.32 %)	2079 (49.74%)	4179 (100 %)
			r_e *too small*	1035 (24.77 %)		

https://doi.org/10.5194/egusphere-2023-2218
Preprint. Discussion started: 16 October 2023

			τ failures	947 (22.66 %)		
18 August 2016, 14:00 UTC	5^o	2344 (96.02%)	r_e too large	46 (1.88 %)	97 (3.97%)	2441 (100 %)
			r_e too small	29 (1.188 %)		
			τ failures	22 (0.90 %)		
	60^o	1368 (56.04%)	r_e too large	339 (13.88 %)	1073 (43.96%)	2441 (100 %)
			r_e too small	178 (7.29 %)		
			τ failures	556 (22.77 %)		

Values in parentheses are percentage of counts. (Percentage of counts = Number of affected pixels/ Total number of pixels)

3.3. Investigating the 3D radiative effects on the Broadband radiative flux

3.3.1. Investigating the 3D radiative effects on the broadband radiative flux: Using a combination of the successful and failed retrievals as the input cloud property

Focusing on SQ3 in this section, we will compare the broadband SW flux results from the 1D-RT + retrieved clouds experiment with those from the 3D-RT + true clouds experiments (i.e., Box E vs. Box F in **Fig. 1**) to investigate the impact of cloud retrieval biases due to the 3D radiative effects on the broadband SW radiative flux. We will also compare results from the 1D-RT + true clouds experiment to those from the 3D-RT + true clouds experiment (i.e., Box F vs. Box G in **Fig. 1**) to study the impact of neglecting horizontal photons transport on the broadband SW flux results.

It is important to note here that both the successful and the failed retrievals as described in Sect. 2.4 are included in the RT simulations in the control simulations presented in this section. The motivation for including the failed retrievals is to preserve the impacts of this significant fraction of pixels on the domain averaged fluxes and CRE simulations, even though the retrieval of τ and r_e based on the bi-spectral method fails for them. In addition to the controlled simulations, we have also conducted sensitivity studies, where we exclude the failed retrievals in the analysis. The results are shown and discussed in the Appendix.

Maps of the simulated SW broadband radiative quantities (reflected flux at the TOD, transmitted flux at the surface, and column absorbed flux) for the 27 June case at the high and low Sun angles are presented in **Fig. 9** and **Fig. 10**, respectively. These figures reveal several interesting and important points. First, it is interesting to note that the reflected flux in **Fig. 9**d seems blurry in comparison with 1D results in **Fig. 9a** and **Fig. 9g**. The same is also seen in **Fig. 10a** and **g**. This is because in 1D RT, simulation of the upwelling hemispheric flux at a given point at the TOD is determined *only* by the cloud and surface properties in the column beneath such point. In contrast, in 3D RT simulation, it depends on the cloud and surface properties of both the corresponding column and a large extent of the surrounding columns, as a result of simple parallax effect. Therefore, the contrast between two adjacent columns in the 1D simulation, for example, a cloudy column and an adjacent clear-sky column next to it, is quite large, whereas the contrast for the same two columns in 3D simulation is much smaller because the two have a significant overlap in terms of the areas that have influences on their flux. Because of this fundamental difference between 1D and 3D simulations, a pixel-to-pixel comparison of the upwelling flux is not appropriate. Instead, we compare the domain-averaged statistics. Before we delve into that, we first aim to unravel how cloud property retrieval errors affect 1D RT flux solutions. For this purpose, we compare the TOD reflected flux as well as the transmitted flux at the surface from the 1D-RT + retrieved clouds and

https://doi.org/10.5194/egusphere-2023-2218
Preprint. Discussion started: 16 October 2023

1D-RT + true clouds experiments (since they are both computed via 1D RT). The TOD reflected flux from the 1D-RT + retrieved clouds experiments have visible signatures of the input cloud property retrievals. For instance, in the high Sun case, smaller reflected flux values (recall, underestimated τ dominates retrievals from high Sun radiance) dominate the reflected flux results from the 1D-RT + retrieved clouds experiment (**Fig. 9a**) as compared to the reflected flux from the 1D-RT + true clouds experiment (**Fig. 9g**). The underestimation of the reflected flux in the 1D-RT + retrieved clouds experiment compared to the 1D-RT + true clouds experiment is evident in **Fig. 9j**. This difference is also well captured in the domain-averaged values which will be discussed later in this section. In the low Sun case, comparison between the reflected flux from the 1D-RT + retrieved clouds experiment and corresponding flux from the 1D-RT + true clouds experiment reveals that in the 1D-RT + retrieved clouds, the overestimated retrieved τ areas characterized by thicker clouds (i.e., retrieved from illuminated pixels) provides larger reflected flux values and the underestimated retrieved τ areas characterized by thinner clouds (i.e., retrieved from shadowed pixels) have smaller reflected flux values than their 1D-RT + true clouds counterpart (**Fig. 10j**). Their overall effect on the domain reflected flux values depends on how the opposite 3D radiative effects (cloud side illumination and shadowing) mitigate each other.

An examination of the transmitted flux at the surface between the 1D-RT + true clouds and 1D-RT + retrieved clouds experiments for the high Sun case reveals that the transmitted flux at the surface beneath clouds in the 1D-RT + retrieved clouds experiment is larger compared to results from the 1D-RT + true clouds experiment, while they have same values in clear-sky regions (**Fig. 9k**). This is expected since the reflected flux from the 1D-RT + retrieved clouds experiment is lesser than results from the 1D-RT + true clouds experiment. Thus, the amount of flux at the surface beneath the cloud in the 1D-RT + retrieved clouds experiment increases. For the low Sun case, the transmitted flux at the surface beneath the clouds in the 1D-RT + true clouds and 1D-RT + retrieved clouds experiments have higher values where the TOD reflected flux is low and lower values where the TOD reflected flux is high (**Fig. 10k**).

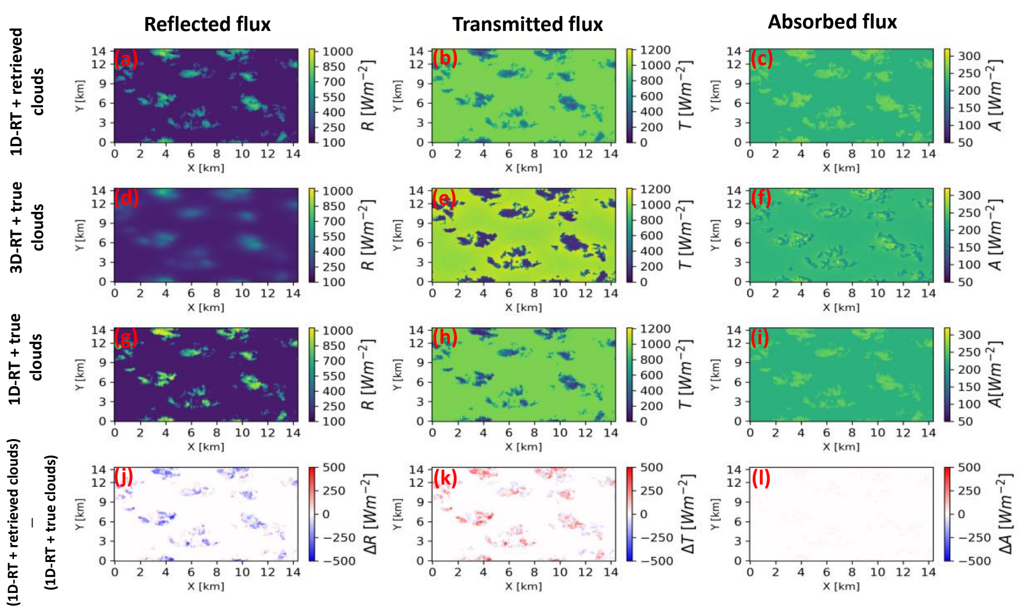

https://doi.org/10.5194/egusphere-2023-2218
Preprint. Discussion started: 16 October 2023

Fig. 9. Simulated shortwave broadband Reflected, Transmitted and Absorbed fluxes for 1D-RT + retrieved clouds (a)-(c), 3D-RT + true clouds (d)-(f), 1D-RT + true clouds (g)-(i) and difference between 1D-RT + retrieved clouds and 1D-RT + true clouds (j)-(l) for Solar zenith angle=5° and View zenith angle=0°. Sun is high and slightly on the Left-hand side of the domain. The solar irradiance at the top of the domain (TOD) scales with the cosine of the Solar zenith angle.

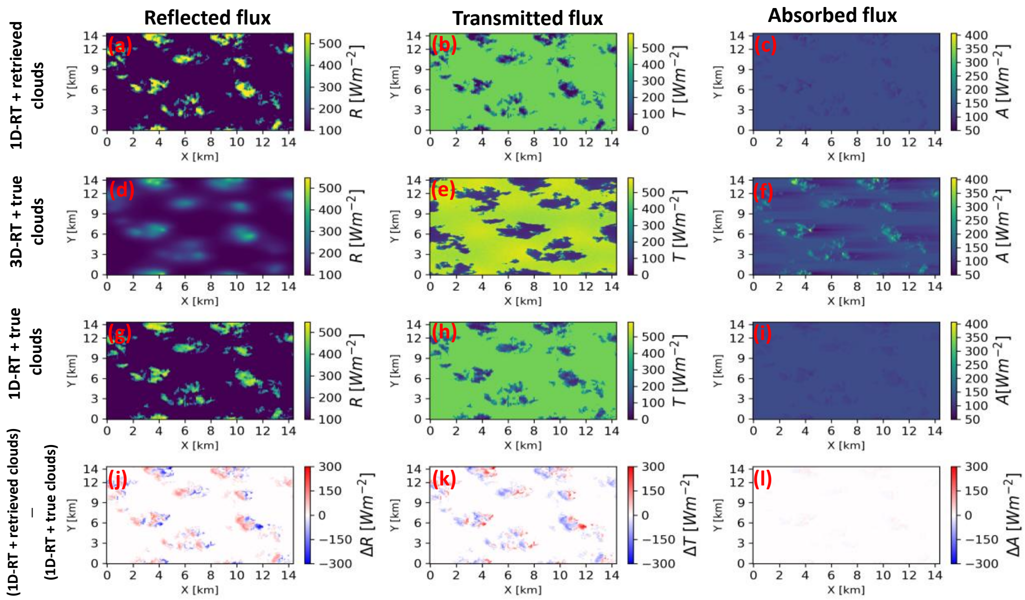

Fig. 10. Simulated shortwave broadband Reflected, Transmitted and Absorbed fluxes for 1D-RT + retrieved clouds (a)-(c), 3D-RT + true clouds (d)-(f), 1D-RT + true clouds (g)-(i) and difference between 1D-RT + retrieved clouds and 1D-RT + true clouds (j)-(l) for Solar zenith angle=60° and View zenith angle=0°, Sun is on the Left-hand side of the domain. The solar irradiance at the top of the domain (TOD) scales with the cosine of the Solar zenith angle.

The radiative quantities across the LES domain have different characteristics in the 3D-RT + true clouds experiment stemming from the horizontal transport of photons across pixels. In the high Sun case of the 3D-RT + true clouds experiment, due to the leaking of photons through cloud sides, the diffused transmitted flux at the surface is larger than results obtained from the 1D-RT + true clouds experiment, similar to the findings made by Wapler and Mayer, [2008]. This is primarily why the transmitted flux at the surface in the high Sun case of the 3D-RT + true clouds experiment is higher than corresponding 1D-RT + true clouds and 1D-RT + retrieved clouds values, especially around cloud edges (**Fig. 9b, e, h**). For the low Sun case of the 3D-RT + true clouds experiment (**Fig. 10e**), due to 3D RT, there is an increase in the total effective cloud cover [Di Giuseppe and Tompkins, 2003; Tompkins and Di Giuseppe, 2007], as well as an increase in the size of the cloud shadow, which reduces the transmitted flux at the surface (e.g., around [X=7,Y=6 km] in **Fig. 10e**). Meanwhile, the cloud shadowed areas projected on the surface shift according to the SZA [Walper and Mayer, 2008; Wissmeier et al., 2013; Jakub and Mayer, 2015, 2017] and are larger for more oblique SZAs.

Table 4. . Domain-averaged broadband shortwave (SW) reflected flux at the top of the domain (R), transmitted flux at the surface (T) and absorbed flux (A) from the 1D-RT + retrieved clouds, 1D-RT + true clouds and 3D-RT + true clouds experiments for the two cloud cases at solar zenith angle (SZA) 5 degrees and SZA 60 degrees.

	SZA 5 degrees	**SZA 60 degrees**

https://doi.org/10.5194/egusphere-2023-2218
Preprint. Discussion started: 16 October 2023

Case Name		*1D-RT + retrieved clouds* (Wm^{-2})	*3D-RT + true clouds* (Wm^{-2})	*1D-RT + true clouds* (Wm^{-2})	*1D-RT + retrieved clouds* (Wm^{-2})	*3D-RT + true clouds* (Wm^{-2})	*1D-RT + true clouds* (Wm^{-2})
27 June 2015 (14:00 UTC)	R	215.44 (213.94)	215.93	225.37 (223.52)	134.22 (111.21)	137.87	133.04 (112.01)
	T	918.97 (920.68)	918.79	910.76 (912.88)	419.60 (441.77)	414.36	420.97 (441.34)
	A	228.56 (228.37)	228.23	226.82 (226.60)	130.25 (131.13)	131.82	130.11 (130.79)
18 Aug. 2016 (14:00 UTC)	R	315.16 (316.82)	308.68	355.26 (357.12)	209.74 (174.40)	218.62	211.54 (171.59)
	T	805.34 (803.59)	812.25	770.21 (768.26)	342.50 (378.46)	326.53	341.92 (382.68)
	A	242.36 (242.48)	241.95	237.36 (237.46)	131.74 (131.20)	138.86	130.55 (129.76)

Note: Values before the parentheses are calculated from the combination of failed and successful retrievals representing the total cloudy population, while values in parentheses are calculated from successful retrievals only representing the total cloudy population. clear-sky pixels values have been included in all calculations.

The domain-averaged broadband reflected flux at the TOD, transmitted flux at the surface, and column absorbed flux values from the 1D-RT + retrieved clouds, 1D-RT + true clouds and 3D-RT + true clouds experiments for the 27 June and 18 August cases at SZA 5° and SZA 60° are reported in **Table 4**. As previously explained, the predominant photon leaking associated with high Sun 3D RT and the ensuing underestimation of the retrieved τ which dominate the cloud property retrievals from high Sun 3D simulated reflectance, increases the number of retrieved optically thinner clouds (relative to the original LES τ used in the 1D-RT + true clouds calculations) utilized as inputs for the 1D-RT + retrieved clouds calculations. This leads to the underestimation of the domain-averaged 1D-RT + retrieved clouds reflected flux compared to the 1D-RT + true clouds reflected flux; In the 27 June case, the domain-averaged reflected flux from the 1D-RT + retrieved clouds experiment (215.44 $\mathrm{Wm^{-2}}$) is underestimated compared to the corresponding 1D-RT + true clouds value (225.37 $\mathrm{Wm^{-2}}$) by about 9.93 $\mathrm{Wm^{-2}}$. While in the 18 August case, the 1D-RT + retrieved clouds experiment underestimates the domain-averaged reflected flux (315.16 $\mathrm{Wm^{-2}}$) compared to the corresponding 1D-RT + true clouds value (355.26 $\mathrm{Wm^{-2}}$) by 40.1 $\mathrm{Wm^{-2}}$. The larger value of the underestimated domain-averaged reflected flux in the 18 August case stems from its larger cloud fraction and τ bias. The transmitted flux at the surface below clouds is dependent on the amount of flux reflected towards the TOD; lower reflected flux values indicate that less radiation is reflected from the clouds, which allows for a greater amount of radiative flux to be transmitted to the surface beneath the clouds. This reason, coupled with the overestimation of the transmitted flux at the surface due to missed thin clouds in our bi-spectral retrievals (red regions in **Fig. 3**, retrieved $\tau = 0$ for VNIR reflectance less than the smallest LUT τ value), explains why for the high Sun case, the domain-averaged values of the surface transmitted flux are higher in the 1D-RT + retrieved clouds experiment compared to the 1D-RT + true clouds values, resulting in differences of 8.21 $\mathrm{Wm^{-2}}$ and 35.13 $\mathrm{Wm^{-2}}$ for the 27 June and 18 August cases respectively. Although, for the high Sun angle, the contribution of the missed thin clouds to the overestimation of the transmitted flux at the surface beneath cloud in our case study is small (Constituting about 0.23% and 0.34% of the domain-averaged surface transmitted flux for the 27 June and 18 August high cases respectively).

Comparing results from the three sets of experiments in **Table 4** reveals that for the high Sun case, the results from the 1D-RT + retrieved clouds clearly agree better with the benchmark 3D-RT + true clouds experiments, than the 1D-RT + true clouds. In the 27 June case, the domain-averaged biases in TOD reflected, surface transmitted and absorbed fluxes for the 1D-RT + retrieved clouds experiment are 0.49, –0.18 and –0.33 $\mathrm{Wm^{-2}}$ respectively, which are significantly smaller in magnitude than those for the 1D-RT + true clouds experiment of –9.44, 8.03, and 1.41 $\mathrm{Wm^{-2}}$ respectively. Similarly, for the 18 August case,

https://doi.org/10.5194/egusphere-2023-2218
Preprint. Discussion started: 16 October 2023

the domain-averaged biases in reflected, transmitted and absorbed fluxes for 1D-RT + retrieved clouds experiment are –6.48, 6.81 and –0.41 Wm^{-2} respectively compared to corresponding biases of –46.58, 42.04, and 4.59 Wm^{-2} for the 1D-RT + true clouds experiments. These results suggests that the 1D-RT + retrieved clouds experiment gives an overall better radiative energy estimate than the 1D-RT + true clouds experiment for the high SZA case. In the low Sun case, the two 1D RT experiments are very close to each other and there is not a clear winner when compared to the benchmark 3D RT results. In the 27 June case, the 1D-RT + retrieved clouds experiment agrees slightly better with 3D results than the 1D-RT + true clouds experiment, but the opposite is true in the 18 August case. This result seems to suggest that although in the low Sun case the illuminating and shadowing effects can lead to large retrieval biases, they tend to cancel out each other in the flux computations. Interesting, both 1D results tend to underestimate the reflected flux and overestimate the transmitted flux. This is probably because the illuminating effect is dominant in the 3D RT leading to some extremely bright pixels. But they are not captured in the 1D experiments, even in the 1D-RT + retrieved cloud experiment using the upper limit of τ=158.48 in the flux computation. Thus, the reflected flux quickly reaches the asymptotic value when τ is large and therefore simply using larger τ value in 1D-RT cannot simulate the extreme brightness of clouds due the illuminating effect in 3D RT.

Because both cloud cases have a cloud fraction lower than 50%, the domain-averaged statistics include a large fraction of clear-sky pixels. Now we focus our scope on cloudy pixels and investigate the differences in CRE. The rCRE bias provides a quantitative estimate of how these biases affect the CRE. For the two cloud cases considered in this study, plots of rCRE bias computed from the reflected flux at the TOD, transmitted flux at the surface and the absorbed flux at SZA 5° and 60° for the 1D-RT + true clouds and 1D-RT + retrieved clouds experiments relative to the 3D-RT + true clouds experiments are presented in **Fig. 11**. In the 27 June case, the rCRE bias of 0.97% computed from the reflected high Sun 1D-RT + retrieved clouds results indicate a negligible deviation (less than 1 %) from the 3D-RT + true clouds CRE while the rCRE bias of −19% computed from the reflected high Sun 1D-RT + true clouds result show that the bias is quite substantial. Similarly, for the 18 August case, the rCRE bias computed from the reflected high Sun 1D-RT + retrieved clouds experiment results is less than 5%. On the other hand, the rCRE bias of −32.48% computed from the reflected high Sun 1D-RT + true clouds result show that the bias is quite large. Similar results are obtained for rCRE bias computed from the surface transmitted flux. In the 27 June case, the rCRE bias computed from the 1D-RT + retrieved clouds transmitted flux is 0.33% (**Fig. 11b**, second bar on the left) which shows minimal bias less than 1%, while the rCRE computed from the 1D-RT + true clouds transmitted flux is −14.5% (**Fig. 11b**, first bar on the left). Similarly, for the 18 August case, the rCRE bias computed from the transmitted 1D-RT + retrieved clouds result is −4.12% (**Fig. 11b**, second bar on the right), while the rCRE bias computed from the transmitted 1D-RT + true clouds result is −25.10% (**Fig. 11b**, first bar on the right).

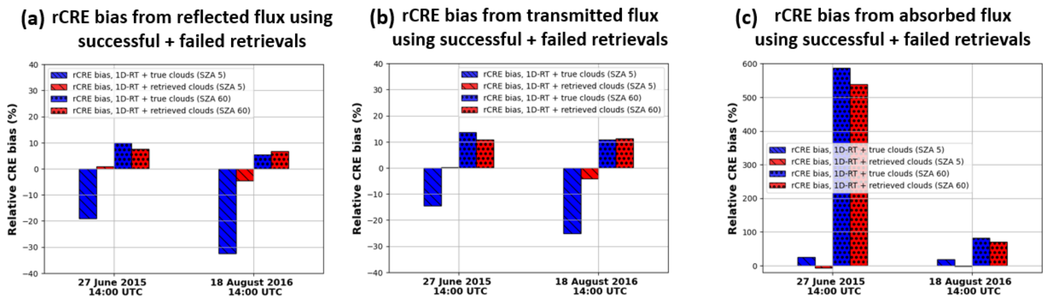

Fig. 11. Relative cloud radiative effect (rCRE) bias computed from the successful + failed retrievals (a) top of the domain reflected, (b) surface transmitted and (c) absorbed flux for the two cloud fields.

When the absorbed flux is taken into consideration, for the 27 June high Sun case, the rCRE bias computed from the absorbed 1D-RT + retrieved clouds flux is −6.05% (**Fig. 11**c, second bar on the left) which is less bias compared to the rCRE bias computed from the absorbed 1D-RT + true clouds flux is 25.64% (**Fig. 11**c, first bar on the left). Similarly, for the 18 August case, the rCRE bias computed from the absorbed 1D-RT + retrieved clouds flux is −1.73% (**Fig. 11**c, second bar on the right), while the rCRE bias computed from the absorbed 1D-RT + true clouds flux is 19.09% (**Fig. 11**c, first bar on the right). For the low Sun case, the rCRE biases from the two 1D-RT experiments are comparable, which is consistent with the domain-averaged statistics in **Table 4**. Evidently, both 1D-RT experiments overestimate the CRE at TOD and surface, which means an underestimation of cloud reflection and overestimation of transmission. This is consistent with the results in **Table 4**.

Overall, the above analysis indicates that the 1D-RT + retrieved clouds experiment provides a better (in the high Sun case) or at least comparable (in the low sun case) results than 1D-RT + true cloud experiment for both domain-averaged flux statistics and CRE when compared to the benchmark 3D-RT results. With these results we can conclude that the despite the potential biases due to 3-D effects the retrieved cloud properties based on 1-D RT from the bi-spectral method still provide a reasonable observational basis to estimate the broadband flux and CRE.

4. Summary and Conclusion

It is well known that the bi-spectral cloud property retrievals based on the 1D-RT have significant errors due to the 3D radiative effects. In this study, we investigate whether the biased retrievals can still be used to estimate the broadband flux and CRE. To address this question, we selected two cloud fields from the LASSO activity: one on 27 June 2015 and another on 18 August 2016 to serve as case studies for our research. The LES cloud fields have different microphysics with different CBH, CTH and the value of the cloud fraction for the 18 August 2016 cloud field (47.08%) is more than twice that of the 27 June 2015 (20.15%) cloud field. Radiance simulations, bi-spectral retrievals, and broadband SW flux radiative transfer simulations were performed using these cloud fields at two SZAs, a high Sun case (SZA=5°) and a low Sun case (SZA=60°) and the results were analyzed. The flux computations were carried out in three sets, the reference broadband SW flux calculations were performed using the cloud properties from the original LES cloud field under 3D RT (we call this the 3D-RT + true clouds experiment), we also computed similar RT broadband SW flux calculations with the same cloud properties from the original LES cloud field except that the RT calculations were computed using 1D RT (we call this the 1D-RT + true clouds experiment).

https://doi.org/10.5194/egusphere-2023-2218
Preprint. Discussion started: 16 October 2023

Additionally, we computed the last set of broadband SW flux calculations using 1D RT and bi-spectrally retrieved cloud properties as inputs (we call this the 1D-RT + retrieved clouds experiment).

The high Sun radiance results, for the two cloud fields show that in 3D RT high Sun case, the photon leaking from optically thick cloudy regions to optically thin cloudy regions dominate the LES reflectance field. These results in overestimated r_e and underestimated τ dominating the cloud property retrievals. While results from the low Sun case, for the two cloud fields considered show that in comparison to the 1D RT radiance fields, illuminating and shadowing effects both occur in the 3D RT simulated radiance observation. Therefore, retrievals from the low Sun 3D radiance observations are characterized mainly by both overestimation of τ and underestimation of r_e in illuminated pixels and underestimation of τ and overestimation of r_e in shadowed pixels. The cumulative effects of these Illuminating and shadowing/Photon leaking effects and its impacts on the retrieved cloud properties dictates their impact on the broadband radiative flux.

The results from the broadband SW radiative fluxes computation showed that although, the bi-spectrally retrieved cloud properties are often biased due to the 3D radiative transfer effects, for high Sun cases, calculations of the CRE from these 1D-RT + retrieved clouds values agree well with the benchmark values (which is the 3D-RT + true clouds experiment in our case) with agreement within 7s% for rCRE bias calculations from the reflected, transmitted and absorbed fluxes in the high Sun cases. Conversely, the rCRE bias computed from the 1D-RT + true clouds flux quantities could reach about 33%. Thus, for high Sun situations, the 1D-RT + retrieved clouds experiment provides consistently better estimates of the CRE than the 1D-RT + true clouds experiment. For the low Sun case, the two 1D RT experiments provide comparable results, both underestimating cloud reflection and overestimating transmission, and there is not a clear winner when compared to the 3D RT benchmark.

The influence of the failed retrievals on the CRE was also investigated (see details in Appendix), with results indicating that for the high Sun case, the impact of the failed retrievals on the radiative flux quantities is negligible, with less than 6% changes observed in the rCRE bias computed from the domain-averaged TOD reflected, surface transmitted and absorbed flux 1D-RT + retrieved clouds and 1D-RT + true clouds experiments. Such is not the case for the low Sun case where the failed retrievals have a very huge impact on the radiative flux quantities. Excluding the failed retrievals from the domain-averaged reflected, transmitted, and absorbed flux 1D-RT + retrieved clouds and 1D-RT + true clouds low Sun case analysis could increase the rCRE bias by a as much as factor of 6 compared to values which included the failed retrievals in the analysis.

In conclusion, despite the potential biases due to the 3D radiative effects, the retrieved cloud properties based on 1D RT from the bi-spectral method still provide a reasonable observational basis to estimate the broadband flux and CRE. Some future questions that warrant answers involves how the 3D radiative effects affect the broadband fluxes for different cloud arrangements and other types of clouds, such as deep convective clouds. Also, while we have considered only nadir view angle in this work, previous studies [e.g., Várnai and Marshak, 2007] have shown that the biases of 1D cloud retrievals vary systematically with view direction, therefore, the impacts of off-nadir view directions on the broadband flux need to be investigated. Another important studies will be to determine how changes in surface albedo and type affects our results. Additionally, while our case study mainly focused on the impact of the 3D radiative effects on SW fluxes, the impact of the 3D radiative effects on LW radiation is important and need to be investigated.

https://doi.org/10.5194/egusphere-2023-2218
Preprint. Discussion started: 16 October 2023

Appendix A: Impacts of failed retrievals on the radiative flux

The 1D-RT + retrieved clouds experiment and domain radiative flux analysis in Sect. 3.3 utilized both the successful and failed retrievals (categorized in Sect. 2.4) to represent the total population of cloudy pixels. Henceforth, both successful and failed retrievals as a representative of the total population of cloudy pixels will be referred to as "all retrieved cloud pixels". In this appendix, our focus is to examine and compare the TOD reflected, surface transmitted and column absorbed radiative fluxes, when the failed retrievals are excluded from the radiative flux analysis. This will help to diagnose if using solely successful retrievals as a representative of the total population of cloudy pixels in the LES domain will produce the correct radiative energy estimates and thus provide information on the radiative properties of the excluded failed retrievals.

An examination of the high Sun domain-averaged TOD reflected, surface transmitted and column absorbed fluxes for both LES cloud cases, when only successful retrievals represent the total population of cloudy pixels in the 1D-RT + retrieved cloud experiment, show minimal changes (within the range $\pm$1.9 $\mathrm{Wm^{-2}}$) from previous values which utilized all retrieved cloud pixels in the radiative flux analysis (**Table 4**). This is due to the small number of failed retrievals in the high Sun scenario (< 14% for both cloud cases; **Table 3**). But this is not the case for the low Sun case, where changes between the two aforementioned calculations are large, reaching up to $\pm$35.96 $\mathrm{Wm^{-2}}$ (**Table 4**). These large changes are because of the large number of failed retrievals from strong 3D radiative effects (> 43% for both cloud cases; **Table 3**) as well as different radiative behavior of the failed retrievals categories observed in the low Sun scenario. **Fig. A1** shows plots of successful and failed retrievals categories (classified as described in Sect. 2.4) from the high and low Sun radiance for the 27 June and 18 August cases. From these plots, it is observed that when the SZA is 60°, the $\mathrm{r_e}$ too small failures are predominant around cloud edges in the sunlit areas. The τ failures are observed mostly in the illuminated sunlit cloudy regions and the $\mathrm{r_e}$ too large failures occur mostly on the opposite sides where the shadowing effect is dominant (**Fig. A1**b and d). For the high Sun at SZA 5°, τ failures are almost negligible because the VNIR reflectance observations does not exceed the LUT τ upper limit of 158.48, while there is a small number of occurrences of the $\mathrm{r_e}$ too large and $\mathrm{r_e}$ too small failures (**Fig. A1**a and c).

It should be noted that when we exclude the failed retrievals from the broadband flux analysis, we keep the total cloud fraction constant. In other words, we scale the broadband flux based on the successful pixels by the ratio of total cloudy to successful pixels such that the effect of cloud fraction reduction is removed from the analysis. The impacts of excluding failed retrievals on the domain-averaged broadband flux can be assessed by comparing the values outside the parentheses with those inside in **Table 4**, and better understood in the light of failed retrieval statistics given in **Table 3**.

Results for the 27 June 1D-RT + retrieved clouds experiment at SZA 5°, show that the domain-averaged TOD reflected flux is underestimated by 1.50 $\mathrm{Wm^{-2}}$ (213.94 $\mathrm{Wm^{-2}}$ in comparison to 215.44 $\mathrm{Wm^{-2}}$) when only successful pixels are used to represent the total population of cloudy pixels compared to results which utilize all retrieved cloud pixels in the radiative flux analysis. This is mainly because the dominant type of retrieval failure in this case is the $\mathrm{r_e}$ too small failure, accounting for about 71% of the failed pixel retrieval statistics (see **Table 3**). Recall that $\mathrm{r_e}$ too small failure is mainly a result of illuminating effect and therefore associated pixels appear brighter in 3D RT than 1D RT. As a result, excluding these pixels leads to an underestimate of domain-averaged broadband reflected flux. For the

https://doi.org/10.5194/egusphere-2023-2218
Preprint. Discussion started: 16 October 2023

same reason, excluding these pixels leads to an overestimation of transmitted flux at the domain bottom .

In contrast to the 27 June case, excluding the failed retrievals in the 18 August case leads to an overestimation of domain-averaged reflected and underestimation of the surface transmitted flux. This is probably because the dominant failed retrieval type is the r_e too large which is because of the shadowing effect. These pixels appear darker from the perspective of TOD and more transmissive from the perspective of bottom in 3D RT than 1D RT. For comparison purpose, we have also excluded the failed pixels from the 1D RT + true clouds. Overall, the results are very similar and consistent with those based on 1D RT + retrieved clouds.

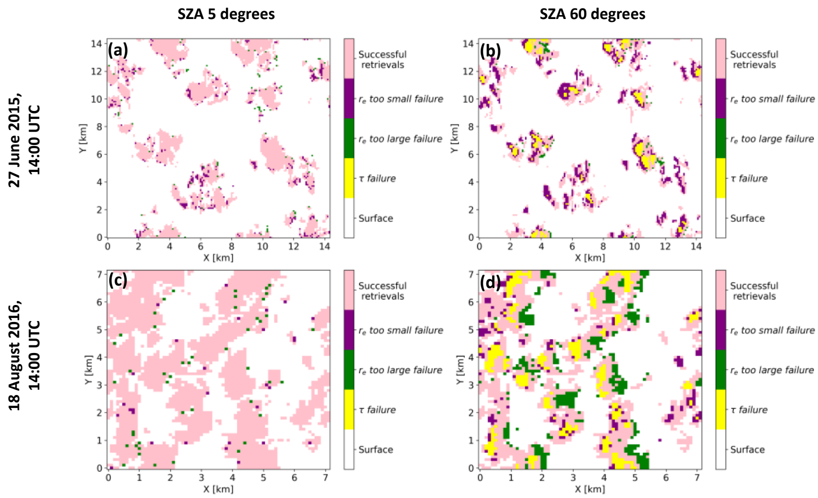

Fig A1. Plots of successful and failed retrievals categories for the 27 June 2015 and 18 August 2016 cases at Solar zenith angle 5 degrees (a and c) and Solar zenith angle 60 degrees (b and d).

In comparison with the high Sun case, the impacts of failed retrievals on the broadband flux statistics are much larger in the low Sun SZA 60° case. In both LES cases, the exclusion of failed retrievals leads to a significant decrease of domain-averaged reflected flux and increase of the transmitted flux. For example, in the 27 June case, the reflected flux decreased from 134.22 $\mathrm{Wm^{-2}}$ when failed pixels are included to 111.21 $\mathrm{Wm^{-2}}$ when they are excluded, which is accompanied by an increase of the transmitted flux from 419.60 $\mathrm{Wm^{-2}}$ to 441.77 $\mathrm{Wm^{-2}}$. A close look at **Table 3** reveals that in both LES cases, the combination of r_e too small and τ failures accounts for the majority of failed retrievals, 95% in the case of 27 June and 68% in the 18 August case. As mentioned above, both types of failures are because of the illuminating effect. Excluding them is expected to cause underestimation of domain-averaged reflected flux and overestimation of transmitted flux.

https://doi.org/10.5194/egusphere-2023-2218
Preprint. Discussion started: 16 October 2023

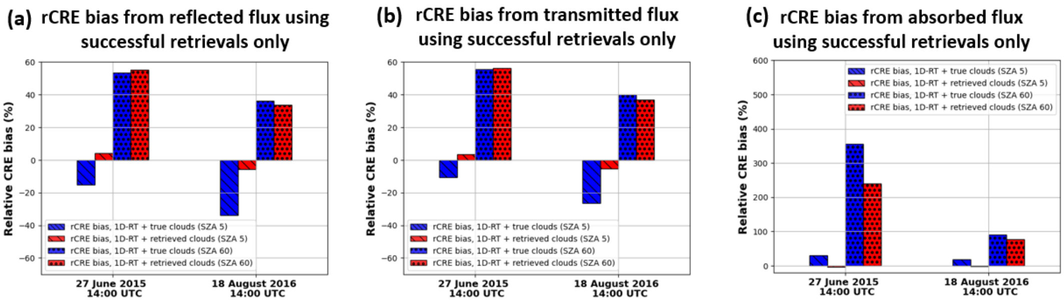

Fig.A2. Relative cloud radiative effect bias computed from the successful only retrievals, top of the domain reflected in (a), surface transmitted in (b) and column absorbed flux in (c) for the two cloud fields.

The impacts of excluding failed retrievals on the rCRE bias are shown in **Fig. A2**. A comparison to the results in **Fig. 11** reveals two points. First the biases in the low Sun cases become much larger which is expected because there are much more failed retrievals in these cases. Second, it is evident that the flux estimates based on 1D-RT + retrieved clouds still provide a better (in case of high Sun) or comparable (in case of low Sun) approximation to the 3D-RT + true clouds simulations in comparison with those based on 1D-RT + true clouds. Therefore, our conclusion made based on the statistics of all retrievals still holds when failed retrievals are excluded from the analysis. On the other hand, it is also evident that to achieve a better comparison with the 3D-RT + true clouds simulations, it is better to include the failed retrievals to preserve the effects of 3D RT.

Author contribution

Conceptualization, Z.Z.; methodology, A.S.A., Z.Z. ; software, A.S.A., Z.Z., ; validation, A.S.A. and Z.Z.; formal analysis, A.S.A.; investigation, A.S.A., and Z.Z.; data curation, A.S.A, Z.Z; writing–original draft preparation, A.S.A.; writing–review and editing, A.S.A.,Z.H.T., J.Z., C.W., S.P., J.W., K.G.M., T.V., Z.Z.; visualization; A.S.A.; supervision, Z.Z.; project administration, Z.Z.; funding acquisition, Z.Z., J.W., K.G.M., C.W. All authors have read and agreed to the published version of the manuscript.

Competing interest

The contact author has declared that none of the authors has any competing interests.

Acknowledgements

This research has been supported by the NASA ACCESS project (grant no. 80NSSC21M0027). The computations for this study have been performed by the UMBC High Performance Computing Facility (HPCF). The facility is supported by the US National Science Foundation through the MRI program (grant nos. CNS-0821258 and CNS-1228778) and the SCREMS program (grant no. DMS-0821311), with substantial support from UMBC.

https://doi.org/10.5194/egusphere-2023-2218
Preprint. Discussion started: 16 October 2023

References

Atmospheric Radiation Measurement (ARM) user facility. 2015. LES ARM Symbiotic Simulation and Observation (LASSO) (LASSODIAGRAW108). 2015-06-27 to 2015-06-27, Southern Great Plains (SGP) Central Facility, Lamont, OK (C1). Compiled by W. Gustafson, A. Vogelmann, X. Cheng, S. Endo, B. Krishna, Z. Li, T. Toto, H. Xiao and K. Johnson. ARM Data Center. Data set accessed 2022-11-08 at http://dx.doi.org/10.5439/1342961.

Atmospheric Radiation Measurement (ARM) user facility. 2016. LES ARM Symbiotic Simulation and Observation (LASSO) (LASSODIAGRAW113). 2016-08-18 to 2016-08-18, Southern Great Plains (SGP) Central Facility, Lamont, OK (C1). Compiled by W. Gustafson, A. Vogelmann, X. Cheng, S. Endo, B. Krishna, Z. Li, T. Toto, H. Xiao and K. Johnson. ARM Data Center. Data set accessed 2023-05-19 at http://dx.doi.org/10.5439/1342961.

Barker, H. W., S. Kato, and T. Wehr (2011), Computation of Solar Radiative Fluxes by 1D and 3D Methods Using Cloudy Atmospheres Inferred from A-train Satellite Data, Surveys in Geophysics, 33(3-4), 657–676, doi:10.1007/s10712-011-9164-9.

Barker HW, Kato S, Wehr T..2012. Computation of solar radiative fluxes by 1D and 3D cloudy atmospheres inferred from A-Train satellite data. *Surv. Geophys*. **33**: 657-676, doi:10.1007/s10712-011-9164-9.

Cho, H. M., Zhang, Z., Meyer, K., Lebsock, M., Platnick, S., Ackerman, A. S., ... & Holz, R. E. (2015). Frequency and causes of failed MODIS cloud property retrievals for liquid phase clouds over global oceans. *Journal of Geophysical Research: Atmospheres*, *120*(9), 4132-4154.

Davis, A. B., & Marshak, A. (2001). Multiple scattering in clouds: Insights from three-dimensional diffusion/P 1 theory. *Nuclear science and engineering*, *137*(3), 251-280.

Di Giuseppe, F., & Tompkins, A. M. (2003). Three-dimensional radiative transfer in tropical deep convective clouds. *Journal of Geophysical Research: Atmospheres*, *108*(D23).

Evans, K.F (1998). The spherical harmonics discrete ordinate method for three-dimensional atmospheric radiative. Journal of the Atmospheric Sciences, 55(3), 429-446.

Gustafson Jr, W. I., Vogelmann, A. M., Li, Z., Cheng, X., Dumas, K. K., Endo, S., ... & Xiao, H. (2020). The large-eddy simulation (LES) atmospheric radiation measurement (ARM) symbiotic simulation and observation (LASSO) activity for continental shallow convection. *Bulletin of the American Meteorological Society*, *101*(4), E462-E479.

IPCC, 2013: *Climate Change 2013: The Physical Science Basis. Contribution of Working Group I to the Fifth Assessment Report of the Intergovernmental Panel on Climate Change* [Stocker, T.F., D. Qin, G.-K. Plattner, M. Tignor, S.K. Allen, J. Boschung, A. Nauels, Y. Xia, V. Bex and P.M. Midgley (eds.)]. Cambridge University Press, Cambridge, United Kingdom and New York, NY, USA, 1535 pp. Ipcc, AR5(March 2013):2014.

Jakub, F., & Mayer, B. (2015). A three-dimensional parallel radiative transfer model for atmospheric heating rates for use in cloud resolving models—The TenStream solver. *Journal of Quantitative Spectroscopy and Radiative Transfer*, *163*, 63-71.

Jakub, F., & Mayer, B. (2017). The role of 1-D and 3-D radiative heating in the organization of shallow cumulus convection and the formation of cloud streets. *Atmospheric Chemistry and Physics*, *17*(21), 13317-13327.

Kato, S., Rose, F. G., Sun-Mack, S., Miller, W. F., Chen, Y. A. N., Rutan, D. A., ... & Collins, W. D. (2011). Improvements of top-of-atmosphere and surface irradiance computations with CALIPSO-, CloudSat-, and MODIS-derived cloud and aerosol properties. *Journal of Geophysical Research: Atmospheres*, *116*(D19).

Kay, J. E., Hillman, B. R., Klein, S. A., Zhang, Y., Medeiros, B., Pincus, R., ... & Ackerman, T. P. (2012). Exposing global cloud biases in the Community Atmosphere Model (CAM) using satellite observations and their corresponding instrument simulators. *Journal of Climate*, *25*(15), 5190-5207.

https://doi.org/10.5194/egusphere-2023-2218
Preprint. Discussion started: 16 October 2023

Kiehl, J. T., & Trenberth, K. E. (1997). Earth's annual global mean energy budget. *Bulletin of the American Meteorological Society*, *78*(2), 197-208.

Loeb, N. G., & Manalo-Smith, N. (2005). Top-of-atmosphere direct radiative effect of aerosols over global oceans from merged CERES and MODIS observations. *Journal of Climate*, *18*(17), 3506-3526.

Liou, K. N. (1992). Radiation and cloud processes in the atmosphere. Theory, observation, and modeling.

Marshak, A., & Davis, A. B. (2005). Horizontal fluxes and radiative smoothing. In *3D Radiative Transfer in Cloudy Atmospheres* (pp. 543-586). Berlin, Heidelberg: Springer Berlin Heidelberg.

Marshak, A., S. Platnick, T. Várnai, G. Wen, and R. F. Cahalan (2006), Impact of three dimensional radiative effects on satellite retrievals of cloud droplet sizes, J. Geophys. Res., 111(D9), D09207, doi:10.1029/2005JD006686.

Masuda, Ryosuke, Hironobu Iwabuchi, Konrad Sebastian Schmidt, Alessandro Damiani, and Rei Kudo. 2019. "Retrieval of Cloud Optical Thickness from Sky-View Camera Images using a Deep Convolutional Neural Network based on Three-Dimensional Radiative Transfer" Remote Sensing 11, no. 17: 1962. https://doi.org/10.3390/rs11171962.

Miller, D. J., Zhang, Z., Ackerman, A. S., Platnick, S., & Baum, B. A. (2016). The impact of cloud vertical profile on liquid water path retrieval based on the bispectral method: A theoretical study based on large-eddy simulations of shallow marine boundary layer clouds. *Journal of Geophysical Research: Atmospheres*, *121*(8), 4122-4141.

Miller, D. J., Zhang, Z., Platnick, S., Ackerman, A. S., Werner, F., Cornet, C., & Knobelspiesse, K. (2017). Comparisons of bispectral and polarimetric cloud microphysical retrievals using LES-Satellite retrieval simulator. *Atmospheric Measurement Techniques Discussions*, *2017*, 1-38.

Mlawer, E. J., Taubman, S. J., Brown, P. D., Iacono, M. J., & Clough, S. A. (1997). Radiative transfer for inhomogeneous atmospheres: RRTM, a validated correlated-k model for the longwave. *Journal of Geophysical Research: Atmospheres*, *102*(D14), 16663-16682.

Morrison, H., & Gettelman, A. (2008). A new two-moment bulk stratiform cloud microphysics scheme in the Community Atmosphere Model, version 3 (CAM3). Part I: Description and numerical tests. *Journal of Climate*, *21*(15), 3642-3659.

Nakajima, T., and M. D. King (1990), Determination of the Optical Thickness and Effective Particle Radius of Clouds from Reflected Solar Radiation Measurements. Part I: Theory, J. Atmos. Sci., 47(15), 1878–1893, doi:10.1175/1520- 0469(1990)047<1878:DOTOTA>2.0.CO;2.

Nam, C., Bony, S., Dufresne, J. L., & Chepfer, H. (2012). The 'too few, too bright'tropical low-cloud problem in CMIP5 models. *Geophysical Research Letters*, *39*(21).

O'Hirok, W., & Gautier, C. (1998). A three-dimensional radiative transfer model to investigate the solar radiation within a cloudy atmosphere. Part I: Spatial effects. *Journal of the Atmospheric Sciences*, *55*(12), 2162-2179.

Okamura, R., Iwabuchi, H., and Schmidt, K. S.: Feasibility study of multi-pixel retrieval of optical thickness and droplet effective radius of inhomogeneous clouds using deep learning, Atmos. Meas. Tech., 10, 4747–4759, https://doi.org/10.5194/amt-10-4747-2017, 2017.

Okata, M., Nakajima, T., Suzuki, K., Inoue, T., Nakajima, T. Y., & Okamoto, H. (2017). A study on radiative transfer effects in 3D cloudy atmosphere using satellite data. *Journal of Geophysical Research: Atmospheres*, *122*(1), 443-468.Doi:10.1002/2016JD025441.

Oreopoulos, L., Cho, N., Lee, D., & Kato, S. (2016). Radiative effects of global MODIS cloud regimes. *Journal of Geophysical Research: Atmospheres*, *121*(5), 2299-2317.

Pincus, R., & Evans, K. F. (2009). Computational cost and accuracy in calculating three-dimensional radiative transfer: Results for new implementations of Monte Carlo and SHDOM. *Journal of the Atmospheric Sciences*, *66*(10), 3131-3146.

Platnick, S., M. D. King, S. A. Ackerman, W. P. Menzel, B. A. Baum, J. C. Riédi, and R. A. Frey (2003), The MODIS cloud products: algorithms and examples from Terra, IEEE TRANSACTIONS ON GEOSCIENCE AND REMOTE SENSING, 41(2), 459–473, doi:10.1109/TGRS.2002.808301.

Platnick, S., Meyer, K. G., King, M. D., Wind, G., Amarasinghe, N., Marchant, B., ... & Riedi, J. (2016). The

https://doi.org/10.5194/egusphere-2023-2218
Preprint. Discussion started: 16 October 2023

MODIS cloud optical and microphysical products: Collection 6 updates and examples from Terra and Aqua. *IEEE Transactions on Geoscience and Remote Sensing*, *55*(1), 502-525.s

Rajapakshe, C., and Z. Zhang (2020), Using polarimetric observations to detect and quantify the three-dimensional radiative transfer effects in passive satellite cloud property retrievals: Theoretical framework and feasibility study, Journal of Quantitative Spectroscopy and Radiative Transfer, 246, 106920, doi:10.1016/j.jqsrt.2020.106920.

Ramanathan, V. L. R. D., Cess, R. D., Harrison, E. F., Minnis, P., Barkstrom, B. R., Ahmad, E., & Hartmann, D. (1989). Cloud-radiative forcing and climate: Results from the Earth Radiation Budget Experiment. *Science*, *243*(4887), 57-63.

Rossow, W. B., & Schiffer, R. A. (1999). Advances in understanding clouds from ISCCP. Bulletin of the American Meteorological Society, 80(11), 2261-2288.

Song, H., Zhang, Z., Ma, P. L., Ghan, S. J., & Wang, M. (2018). An evaluation of marine boundary layer cloud property simulations in the Community Atmosphere Model using satellite observations: Conventional subgrid parameterization versus CLUBB. *Journal of Climate*, *31*(6), 2299-2320.

Stephens, G. L. (1977). The transfer of radiation through vertically nonuniform stratocumulus water clouds. *Radiation in the Atmosphere*, 184.

Tompkins, A. M., & Di Giuseppe, F. (2007). Generalizing cloud overlap treatment to include solar zenith angle effects on cloud geometry. *Journal of the atmospheric sciences*, *64*(6), 2116-2125.

Trenberth, K. E., Fasullo, J. T., & Kiehl, J. (2009). Earth's global energy budget. *Bulletin of the american meteorological society*, *90*(3), 311-324.

Trishchenko, A. P., Luo, Y., Cribb, M., Li, Z., & Hamm, K. (2003). Surface spectral albedo intensive operational period at the ARM SGP site in August 2002: Results, analysis, and future plans. In *Proceedings of the Thirteenth Atmospheric Radiation Measurement (ARM) Program Science Team Meeting, US Department of Energy, Richland, Washington*.

Vardavas, I., & Taylor, F. (2011). *Radiation and Climate: Atmospheric energy budget from satellite remote sensing* (Vol. 138). International Monographs on Ph.

Várnai, T., and R. Davies (1999), Effects of Cloud Heterogeneities on Shortwave Radiation: Comparison of Cloud-Top Variability and Internal Heterogeneity, *J. Atmos. Sci.*, *56*(24), 4206–4224, doi:10.1175/1520-0469(1999)056<4206:EOCHOS>2.0.CO;2.

Várnai, T. (2000). Influence of three-dimensional radiative effects on the spatial distribution of shortwave cloud reflection. *Journal of the atmospheric sciences*, *57*(2), 216-229.

Várnai, T., Marshak, A., & Lau, W. K. (2001). Observations of three-dimensional radiative effects that influence satellite retrievals of cloud properties.

Várnai, T., & Marshak, A. (2002). Observations of three-dimensional radiative effects that influence MODIS cloud optical thickness retrievals. *Journal of the Atmospheric Sciences*, *59*(9), 1607-1618.

Várnai, T., & Marshak, A. (2007). View angle dependence of cloud optical thicknesses retrieved by Moderate Resolution Imaging Spectroradiometer (MODIS). *Journal of Geophysical Research: Atmospheres*, *112*(D6).

Wapler, K., & Mayer, B. (2008). A fast three-dimensional approximation for the calculation of surface irradiance in large-eddy simulation models. *Journal of Applied Meteorology and Climatology*, *47*(12), 3061-3071.

Welch, R. M., & Wielicki, B. A. (1984). Stratocumulus cloud field reflected fluxes: The effect of cloud shape. *Journal of the atmospheric sciences*, *41*(21), 3085-3103.

Wielicki, B. A., Barkstrom, B. R., Harrison, E. F., Lee III, R. B., Smith, G. L., & Cooper, J. E. (1996). Clouds and the Earth's Radiant Energy System (CERES): An earth observing system experiment. *Bulletin of the American Meteorological Society*, *77*(5), 853-868.

Wissmeier, U., Buras, R., & Mayer, B. (2013). paNTICA: A fast 3D radiative transfer scheme to calculate surface solar irradiance for NWP and LES models. *Journal of applied meteorology and climatology*, *52*(8), 1698-1715.

Zelinka, M. D., Klein, S. A., & Hartmann, D. L. (2012). Computing and partitioning cloud feedbacks using

https://doi.org/10.5194/egusphere-2023-2218
Preprint. Discussion started: 16 October 2023

cloud property histograms. Part II: Attribution to changes in cloud amount, altitude, and optical depth. *Journal of Climate*, *25*(11), 3736-3754.

Zhang, Z., & Platnick, S. (2011). An assessment of differences between cloud effective particle radius retrievals for marine water clouds from three MODIS spectral bands. *Journal of Geophysical Research., 116, D20215, doi:10.1029/2011JD016216.*

Zhang, Z., A. S. Ackerman, G. Feingold, S. Platnick, R. Pincus, and H. Xue (2012), Effects of cloud horizontal inhomogeneity and drizzle on remote sensing of cloud droplet effective radius: Case studies based on large-eddy simulations, J Geophys Res, 117(D19), D19208–, doi:10.1029/2012JD017655.

Zhang, Z., F. Werner, H. M. Cho, G. Wind, S. Platnick, A. S. Ackerman, L. Di Girolamo, A. Marshak, and K. Meyer (2016), A framework based on 2-D Taylor expansion for quantifying the impacts of sub-pixel reflectance variance and covariance on cloud optical thickness and effective radius retrievals based on the bi-spectral method, Journal of Geophysical Research-Atmospheres, 2016JD024837, doi:10.1002/2016JD024837.

Zhang, Z., Dong, X., Xi, B., Song, H., Ma, P. L., Ghan, S. J., ... & Minnis, P. (2017). Intercomparisons of marine boundary layer cloud properties from the ARM CAP-MBL campaign and two MODIS cloud products. *Journal of Geophysical Research: Atmospheres*, *122*(4), 2351-2365.

Zhuravleva, T. B., Kabanov, D. M., Sakerin, S. M., & Firsov, K. M. (2009). Simulation of aerosol direct radiative forcing under typical summer conditions of Siberia. Part 1. Method of calculation and choice of input parameters. *Atmospheric and Oceanic Optics*, *22*, 63-73.